The Raman LIDAR technique

Marco Iarlori

marco.iarlori@univaq.it

Center of Excellence CETEMPS
Telesensing of Environment and Model Prediction of Severe events

INFN
Istituto Nazionale di Fisica Nucleare

DSFC
Dipartimento di Scienze Fisiche e Chimiche

Outline:

- **Brief Historical background.**
- **The Elastic/Raman Lidar equation & why we need a Raman Lidar**
- **The retrieval of the aerosol optical parameters and water vapor.**
- **Details on the aerosol extinction retrieval.**
- **Quality assurance tools & brief uncertainties discussion.**

The rapid development of modern lidar technology started with the invention of the laser in 1960 and the giant-pulse or Q-switched laser in 1962.

Fiocco and Smullin published atmospheric observations with a ruby laser in 1963. About a decade later all basic lidar techniques had been suggested and demonstrated.

Ulla Wandinger "Raman Lidar" in "Lidar Range-Resolved Optical Remote Sensing of the Atmosphere" Springer 2005.

magnetic wave modes, the corresponding mode velocities are 1,700 and 450 km/sec. Both these values are about 40 per cent lower than those reported for the Argus tests of 1958[4,5]. In connexion with the 2·5-sec delay observed for one component of the October 26 signature, we point out that Roquet *et al.*[6] have shown that the main phase of the signature from the July 9 test showed a world-wide delay of about 2 sec following the instant of detonation. Reports from other observers on observations of the later American tests may provide further evidence of this important effect. The paucity of published results on the electro-magnetic effects of the October–November 1962 tests, relative to the July 9 test, is due no doubt to the more spectacular nature of the latter. We suggest, however, that attention devoted to the results of the October–November series may prove equally rewarding.

A fuller account of this work is being prepared for publication elsewhere.

R. A. SANTIROCCO
D. G. PARKER

Research Department,
General Dynamics/Electronics,
Rochester, New York.

[1] Ashburn, E. V., Lee, J. P., and Francis, R. N., *J. Geophys. Res.*, **67**, 4933 (1962).
[2] Crain, C. M., and Tamarkin, P., *J. Geophys. Res.*, **66**, 35 (1961).
[3] Zmuda, A. J., Shaw, B. W., and Haave, C. R., *J. Geophys. Res.*, **68**, 745 (1963).
[4] Berthold, W. K., Harris, A. K., and Hope, H. J., *J. Geophys. Res.*, **65**, 2233 (1960).
[5] Bomke, H. A., Ramm, W. J., Goldblatt, S., and Klemas, V., *Nature*, **185**, 299 (1960).
[6] Roquet, J., Schlich, R., and Selzer, E., *J. Geophys. Res.*, **68**, 3731 (1963).

Detection of Scattering Layers in the Upper Atmosphere (60–140 km) by Optical Radar

THIS communication reports observations made by us of optical echoes from atmospheric constituents (presumably dust) at heights of 60–140 km. They were detected with an optical radar. The techniques utilized are a development of those already reported by us[1,2].

The optical radar consists of an RCA-designed ruby laser delivering short pulses of approximately 50 nsec, 0·5 joule at $\lambda = 6{,}940$ Å; of a transmitting refracting telescope of 7·5-cm diameter and 201-cm focal length; of a receiving reflecting telescope of 32-cm diameter and 270-cm focal length, and of a photometer utilizing a 20-Å wide interference filter and a cooled EMI 9,558 *A* photomultiplier. The two telescopes are accurately boresighted and rigidly connected on an equatorial mount. All observations reported here were made with the telescopes looking at the zenith. Each time that the laser was fired the return signals picked up by the photomultiplier were displayed on an oscilloscope and photographed. The return signals originating above 30 km were so weak that it was possible to count individual photoelectrons in each 10-km (66-μsec) interval up to 180 km. These experiments were carried out during the months of June and July 1963 at Lexington, Massachusetts. They show the Rayleigh molecular scattering at heights up to 50–60 km. At greater heights—up to 140 km—very weak echoes were detected which we ascribe to dust clouds. These latter echoes appear to come from two main regions: 60–90 km (often about 80 km) and 110–140 km (often about 120 km).

Fig. 1 shows the results of the observations of four consecutive days, July 28–31. This interval covers the period of the δ-Aquarids meteor shower. The sums of the photoelectrons obtained in successive 10-km range intervals are displayed for each night. The large initial counts, resulting from molecular Rayleigh scattering, permit an independent calibration of the apparatus. The noise-level, which is represented by photomultiplier dark current and sky background, is established by taking the average of the returns in the interval 140–180 km. Independent noise measurements taken between laser firings were in substantial agreement with those taken from the extreme ranges. Since the noise has the character of a Poisson process, the standard deviation is taken to be $\sqrt{n}$, where n is the average noise-level count per range-interval; note that the peaks obtained on July 30 and 31 exceed the average noise-level by more than 3 times the standard deviation.

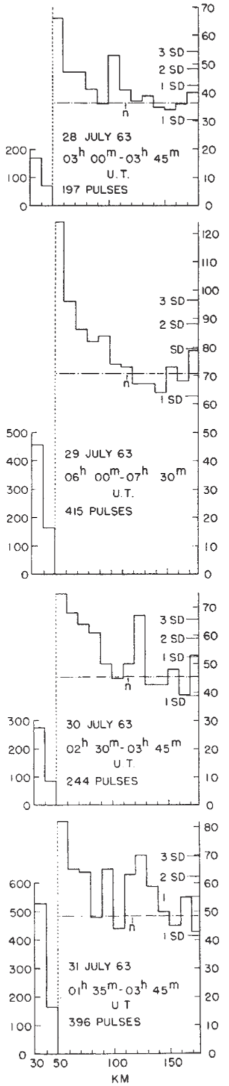

Fig. 1. Accumulated photoelectron counts in 10-km range intervals for July 28–31, 1963; n is the average noise-level

Many similar sets of data have been collected that show similar behaviour. Table 1 was compiled after a preliminary analysis of 9 days of observation. The X's show the occurrence of peaks exceeding the average noise-level by a factor of $3\sqrt{n}$. The echoes obtained on July 31 correspond to a backscattering differential cross-section per unit volume (averaged between 120 and 130 km) of $2 \cdot 10^{-13}$ cm^{-1} steradians^{-1}.

Table 1. OCCURRENCE OF ECHOES ON NINE NIGHTS OF OBSERVATION

U.T. (1963)	Range (km) 60		70		80		90		100		110		120		130		140
July 17						X						X		X			
July 24		X															
July 25					X	X											
July 26		X															
July 27												X					
July 28																	
July 29																	
July 30														X			
July 31														X			

In the absence of independent methods of observation we cannot say what causes these echoes. However, one is tempted to compare the lower echoes (~80 km) with the observed heights of noctilucent clouds. It has been speculated that more distant echoes (~120 km) correspond to the region of meteoric break-up.

The assistance of F. W. Barrows, H. B. Gay, G. A. Garosi, and G. S. Misail in the construction of the apparatus and of H. C. McClees in the conduct of the experiment is gratefully acknowledged. We thank Prof. A. H. Barrett for many helpful discussions. This work was supported in part by the U.S. Army, the Air Force Office of Scientific Research, and the Office of Naval Research; and in part by the National Aeronautics and Space Administration (Grant *NsG*–419).

G. FIOCCO
L. D. SMULLIN

Department of Geology and Geophysics,
Department of Electrical Engineering and
Research Laboratory of Electronics,
Massachusetts Institute of Technology,
Cambridge, Mass.

[1] Smullin, L. D., and Fiocco, G., *Nature*, **194**, 1267 (1962); *Proc. Inst. Radio Eng.*, **50**, 1703 (1962).
[2] Fiocco, G., and Thompson, E., *Phys. Rev. Letters*, **10**, 89 (1963).

The Raman lidar technique makes use of the weak inelastic scattering of light by atmospheric molecules. The excitation of a variety of rotational and vibrational molecular energy levels leads to several bands of Raman scattered radiation the frequency shifts of which are characteristic for the interacting molecule.

Ulla Wandinger "Raman Lidar" in "Lidar Range-Resolved Optical Remote Sensing of the Atmosphere" Springer 2005.

LETTERS TO THE EDITOR

PLANETARY SCIENCE

Observation of Raman Scattering from the Atmosphere using a Pulsed Nitrogen Ultraviolet Laser

THIS communication reports the experimental observation of optical Raman scattering from oxygen and nitrogen in the atmosphere using a pulsed nitrogen ultraviolet laser[1,2] as a light source. Previous atmospheric laser scattering experiments have been reported[3,4] which utilized Rayleigh scattering or scattering from particulate matter such as aerosols and dust particles. With Raman scattering, the wavelength of the scattered light is shifted, the amount of the shift being specific to the scattering molecule. The importance of the Raman scattering technique is that it enables a range resolved measurement of atmospheric constituents, with respect to both species and concentration, from a single remote location. This type of measurement could be useful in such fields as meteorology, atmospheric physics and air pollution control.

The apparatus used in the Raman scattering experiments is shown in Fig. 1. The transmitter consisted of an uncollimated 100 kW peak power, 10 nsec, 3371 Å pulsed nitrogen laser (Avco model *C*-102). A 20 cm diameter, 1·6 m focal length telescope and an RCA 7265 photomultiplier with an *S*-20 cathode response served as the receiver. Continuous wavelength selection was obtained by tilting interference filters away from normal incidence. Two interference filters were used, each with a transmission band width of 35 Å at half maximum. The transmissions for these filters were centred at 3557 Å and 3658 Å for normal incidence. A maximum filter tilt angle of 35° was possible with the apparatus, yielding a maximum wavelength shift of approximately 200 Å. The experiment was conducted at Everett, Massachusetts, at times shortly after sunset during July 1967.

A spectral analysis of the experimentally obtained air scattering return at zero elevation is shown in Fig. 2. In addition to the strong return at the 3371 Å transmitter wavelength, signals, weaker by about a factor of 1,000,

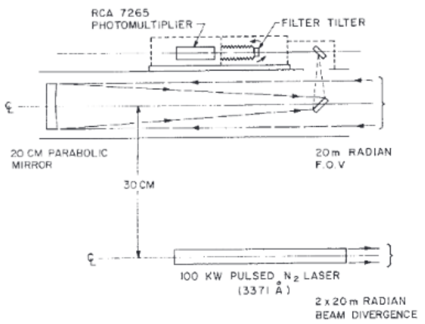

Fig. 1. Schematic diagram of the apparatus used to observe atmospheric Raman scattering.

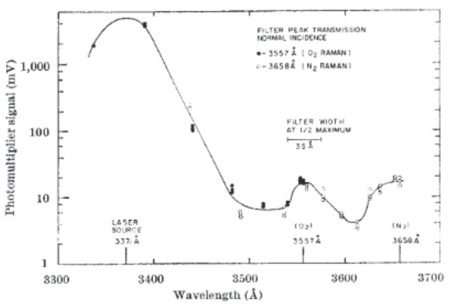

Fig. 2. Photomultiplier signal from atmospheric backscatter as a function of wavelength. Each data point represents a single measurement obtained with one laser pulse.

were observed at 3557 Å and 3658 Å, corresponding to the vibrational Raman shift for oxygen and nitrogen, respectively. The magnitude of the observed Raman signals was consistent with the expected signal calculated on the basis of an estimated Raman cross-section of 10^{-29} cm². Measurements of this type can be used to obtain directly the oxygen to nitrogen concentration ratio as a function of range.

The apparent spectral width of the experimental backscatter signal in Fig. 2 near the laser line at 3371 Å is thought to result from the rejection properties of the interference filter. This was determined by comparing the air backscatter near 3371 Å with the return from a solid target. No significant difference, as a function of wavelength, was observed when the target signals were normalized to the air backscatter.

It is hoped that, with improvements in both resolution and rejection, Raman signals can be observed in this wavelength region from other sources. Signals originating from rotational transitions in oxygen and nitrogen, infrared transitions in various atmospheric contaminants, and vibrational transitions in small solid air-borne particles are of particular interest.

Typical oscillograms of the photomultiplier signal, obtained at the 3658 Å nitrogen Raman line, are shown in Fig. 3. At the beginning the observed pulse shape is dominated by the non-coaxial transmitter-receiver geometry. When the fields of view of the transmitter and receiver have sufficiently overlapped, the signal decay can be fitted to an inverse squared law multiplied by an exponential extinction. The signals shown in Fig. 3 yield useful data for up to 8 µsec, which corresponds to a range of 1·2 km. The application of photon counting methods, with p[illegible]onds, should greatly [illegible] same laser transm[illegible]

A ra[illegible]tered power in the [illegible]wn[5] to yield directly [illegible]he range of interes[illegible]n scattering may [illegible]smissometer applic[illegible]nded transmissom[illegible]e knowledge of the [illegible]er from the suspended particles, causing the reduced visibility, and the transmission through them, and relied therefore on an analysis of the backscatter pulse shape, rather than a simple power measurement.

The 3371 Å pulsed nitrogen laser was chosen from among the available strong laser sources for the following reasons. Raman scattering cross-sections vary inversely with the fourth power of the incident wavelength. Thus the pulsed nitrogen laser is more effective than a ruby laser by a

D.A. Leonard
Nature 216,
142 (1967)

Measurements Separating the Gaseous and Aerosol Components of Laser Atmospheric Backscatter

THIS article describes preliminary results of laser atmospheric backscatter measurements which use both the frequency shifted Raman scatter and unshifted Rayleigh components of the returns to separate the returns due to gaseous constituents from those due to aerosol constituents of the atmosphere.

Observations of the frequency shifted (Raman component) of laser atmospheric backscatter off the vibrational levels of N_2 have already been reported[1]. By preferentially rejecting the backscatter return at 6943 Å in the vicinity of the Rayleigh line, the return of the Raman component from N_2 due to the band centred at 8283 Å can be monitored quite easily even though the Rayleigh/Raman cross-section ratio is ≃500. The intensity of the backscatter at 8283 Å depends only on the local density of nitrogen molecules (except for transmission losses) whereas the return at 6943 Å contains both the gaseous and aerosol backscatter in ambiguous proportion. In conditions of poor visibility the ambiguity in the return signal can be relatively small due to the preponderance of the aerosol return, but during good visibility the ambiguity is large. With essentially simultaneous backscatter returns at both 6943 Å and 8283 Å, a simple subtraction permits the identification of that fraction of the 6943 Å return due to aerosol scatter.

When monitoring the Raman component at 8283 Å, rejection of the 6943 Å light by a factor of 10^8 is provided by a combination of optical pass band and rejection filters. A neutral density filter with a transmission of 3×10^{-4} at 6943 Å is interposed in the optical path of the receiver when monitoring the 6943 Å backscatter in order to reduce the system output to that which occurs when monitoring the Raman signal. Calibration of the receiver system showed that the 6943 Å returns have to be reduced by 0·72 for quantitative comparisons with the 8283 Å returns.

The results of the combined 6943–8283 Å data fall into two general categories: (1) no pronounced scatter discontinuity, shown by the relative smoothness of the 6943 Å

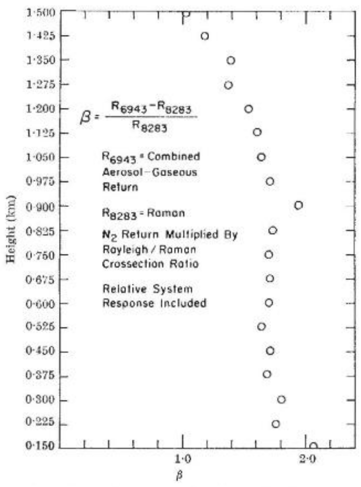

Fig. 1. Normalized cross-section of aerosol backscatter.

returns and substantiated by the 8283 Å returns; (2) a pronounced scatter discontinuity on the 6943 Å return accompanied by a complete absence of a similar effect on the 8283 Å returns.

One hundred and sixty oscilloscope traces were recorded of the roughly three hundred observations. A typical category 1 result is shown in Fig. 1 where the aerosol to gaseous backscatter ratio is plotted. Although low backscatter ratios such as in Fig. 1 have been measured before, Fig. 1 is none the less surprising in terms of the usual aerosol models (the Junge size distribution, for example). For a Junge distribution with exponent $\nu = 3·5$, the average differential scatter to backscatter ratio is about 5·0. Thus even with a 20 km visibility parameter, one expects a factor of about 6·0 for the aerosol to gas backscatter ratio. A factor of 4·0 is the upper limit on the present measurements. A 20 km visibility parameter corresponds to a very clear day for the eastern US seaboard and is not at all typical. Hazier weather would yield ratios larger than 6·0. These data suggest a larger anisotropy corresponding to a significant variation from the models. We are reducing the size of the absolute error to discover the nature of the discrepancy between the measurements and aerosol models.

The absolute value of the ratio can be in error by no more than a factor of about two. This is due primarily to the uncertainty in the Raman/Rayleigh cross-section ratio. The relative error (shot-to-shot system response) is less than 5 per cent, based on the repeatability of the N_2 return. This repeatability implies a relatively high accuracy for the vertical gradients in the backscatter return.

Fig. 2—a direct copy of a Polaroid film—gives a typical result from the second category of data. The dotted curve clearly shows the discontinuity in the 6943 Å return, while the Raman return (solid curve), taken at ≃30 s later, shows no evidence of the discontinuity. The discontinuity was a return from a somewhat localized semitransparent cloudlike layer, and by orienting the optic axis of the system out of the line of sight of the layer, 6943 Å returns were obtained in which there was no discontinuity. This shows very clearly that the N_2 Raman returns are quite insensitive to the presence of aerosols and so provide a useful means of deducing the amount of aerosol contribution to the backscatter in Rayleigh returns. On some of the N_2 returns there was an indication of a small discontinuity at the same altitude as the pronounced discontinuity on the 6943 Å returns, but these discontinuities have not been statistically validated.

The altitude range of the system is limited by the Raman retu[illegible]ble signal/noise ratios.[illegible]itter and receiver ax[illegible]ignals for the altitude[illegible]o be more interesting.[illegible]normalizing out" the[illegible]assuming an exact 1/[illegible]

We also [illegible]g the so-called on–o[illegible]e spectral purity of th[illegible]frequency slightly rem[illegible]band were inserted in [illegible]data compared with [illegible] intensity ratios are [illegible]periments could verify[illegible]s (such as light leaks) [illegible]sults show that leaks [illegible], causing an undesirable enhancement of the 8283 Å signal, range from 0·71 per cent to 5·9 per cent. But the leaks can be ignored because of the larger error associated with the uncertainty in the Raman/Rayleigh cross-section ratio.

By using ground measurements of pressure and temperature plus assumed lapse rates, it might be possible to extract from the 6943 Å return alone, simply by calcula-

J. Cooney
J. Orr
C. Tomasetti:
Nature 224,
1098 (1969)

Observation of Raman Scattering by Water Vapor in the Atmosphere

Show affiliations

Melfi, S. H. ; Lawrence, J. D., Jr. ; McCormick, M. P.

First measurement of the water vapor profile with the Raman technique

Raman backscatter of a frequency-doubled ruby laser beam by water vapor has been observed in the atmosphere, using an optical radar system. This return along with a Raman nitrogen return, has been used to calculate a relative water-vapor mixing ratio profile in the atmosphere to an altitude of approximately 2 km.

Publication: Applied Physics Letters, Volume 15, Issue 9, p.295-297

Pub Date: November 1969

DOI: 10.1063/1.1653005

Bibcode: 1969ApPhL..15..295M

A67-41027 #

AIRPORT GLIDE SLOPE VISUAL RANGE INDICATOR.

E. T. Gerry and D. A. Leonard (Avco Corp., Avco-Everett Research Laboratories, Everett, Mass.).

(Congrès International sur les Applications des Lasers, 1st, Paris, France, July 18-23, 1967, Communication.)

Lasers, no. 7, 1967, p. 47, 48. 6 refs.

Description of a glide-slope transmissometer (which is essentially an optical radar in which the receiver is gated on to receive signals from only a specified range interval and is tuned to a wavelength other than the transmitted wavelength). The device measures the two-way transmission through the atmosphere between the receiver and a light source of known intensity situated at a known distance from the receiver. The light source is a laser emitting a short pulse of monochromatic light in the direction where the visibility is to be measured. The receiver is a gated photodetector tuned to the light wavelength corresponding to vibrational Raman scattering of the incident laser beam from a component of air. The time delay before the receiver is gated on specifies the range at which the measured scattering occurs.

E.T. Gerry, D.A. Leonard: Airport glide slope visual range indicator using laser Raman scattering. Proceedings, First International Conference on Laser Applications, Paris, France, 1967

First attempts to infer particle extinction properties from Raman signal profiles

1 February 1974

A Single-ended Atmospheric Transmissometer

Donald A. Leonard, Bernard Caputo

Author Affiliations +

Optical Engineering, Vol. 13, Issue 1, 130110 (February 1974). https://doi.org/10.1117/12.7971669

First accurate measurement of the horizontal transmission with the Raman technique

Abstract

It has been shown experimentally that a measurement of the Raman shifted component of the laser backscatter from atmospheric nitrogen will give a direct determination of transmission as a function of range. This type of single-ended device, when operating in a radar-like mode, can satisfy the need to accurately measure atmospheric transmission. A major difficulty in the interpretation of pulsed lidar backscatter data is that unless a priori information is available concerning the relationship between the volume backscattering coefficient and the attenuation coefficient, the received intensity cannot be easily evaluated as transmittance. The backscatter coefficient for Raman scattering, however, depends only on the Raman cross-section of the specific molecule used and the number density of that molecule. In the lower atmosphere the density of atmospheric nitrogen is constant. A measurement of Raman scattering from nitrogen will therefore give a direct determination of transmission as a function of range. Experiments were conducted over a 1/4-mile range and produced consistent results for transmissions down to as low as 2 percent when compared with simultaneous double-ended reference transmissometer data. The laser Raman transmissometer system is now computer controlled and produces real time data displays.

Raman Lidar become more common in the 90s also because the Pinatubo eruption (1991) caused problems to the standard Lidar based Stratospheric Ozone measurements (elastic DIAL technique))

RAMAN DIAL MEASUREMENTS OF STRATOSPHERIC OZONE IN THE PRESENCE OF VOLCANIC AEROSOLS

Thomas J. McGee[1], Michael Gross[2], Richard Ferrare[2], William Heaps[1], and Upendra Singh[2]

Abstract. Since the eruption of Mt. Pinatubo in June, 1991, measurements of atmospheric species which depend on Rayleigh scattering of radiation, have been severely compromised where the volcanic aerosol cloud exists. For the GSFC stratospheric ozone lidar, this has meant that ozone determination has been impossible below approximately 30 km. The GSFC lidar has been modified to detect Raman scattering from nitrogen molecules from transmitted laser wavelengths. The instrument transmits two laser wavelengths at 308 nm and 351 nm, and detects returns at four wavelengths; 308 nm, 332 nm, 351 nm, and 382 nm. Using this technique in conjunction with the Rayleigh DIAL measurement, ozone profiles have been measured between 15 and 50 km.

Introduction

Measurements of stratospheric ozone by the Differential Absorption Lidar (DIAL) technique have become commonplace during the last several years (McGee et al., 1991; McDermid et al., 1990; Uchino, et al., 1983; Pelon et al., 1986; Browell, 1989). Indeed, the International Network for the Detection of Stratospheric Change intends to place such instruments at each of their selected research stations.

The DIAL technique for the measurement of ozone consists of the transmission of at least two wavelengths into the atmosphere, one wavelength which is absorbed by ozone and another which is significantly less absorbed. Radiation at these two wavelengths is scattered by the atmosphere and collected by a telescope aligned with the transmitted beams. The majority of the systems mentioned above, particularly the instruments designed for stratospheric measurements, use excimer lasers transmitting at 308 and 353 nm for the "on" and "off" line wavelengths. In a clean atmosphere, the scattering mechanism is almost entirely Rayleigh, and the wavelength dependence of Rayleigh scattering is well-known. In this case the effect of aerosols can be either ignored or a small correction applied. In the circumstance in which the stratosphere is injected with a fresh influx of volcanic SO_2, the sulfuric acid aerosol content of the stratosphere changes rapidly, both in particle size distribution and concentration. Without accurate information about the composition and size distribution of the aerosols it is impossible to know the wavelength dependence of the Mie scattering. Therefore, with a lidar which has wavelengths as widely separated as those which are common in the stratospheric systems (Megie and Menzies, 1980), it is virtually impossible to extract an ozone profile in the regions where Mie scattering has "contaminated" the lidar return. (There are some other lidar systems which measure ozone using wavelengths which are not so widely spaced [see for example Browell et al. 1990]. In those cases, the errors introduced because of aerosols would be considerably reduced. Those lidar systems do not, however, have the high altitude capability of the large ground based stratospheric system). Figure 1 shows a plot of the Aerosol Backscattering Ratio [(Rayleigh + Mie)/Rayleigh] obtained as a function of altitude. This plot is extracted from an inversion of the lidar return of the "off-line" (or unabsorbed) wavelength. The density of the atmosphere is obtained from a local radiosonde. The Backscatter Ratio is the ratio of the measured lidar return to the calculated Rayleigh return based on the known atmospheric molecular density. Data from before and after the eruption of Mt. Pinatubo are plotted. The effect of such large aerosol loadings on the Rayleigh DIAL measurement of ozone is seen in Figure 2. Because of this interference from aerosol scattering, recent measurements of ozone have been impossible below 30-32 km.

Also included in Figure 2 is an attempt to correct the profile for scattering and extinction due to aerosols. It is clear that our assumptions for volcanic aerosols are incorrect. There is insufficient information about the aerosol parameters to make a viable correction. This is especially true in the period shortly after a major eruption as the concentration, composition and size of the particles are changing rapidly.

The knowledge that HNO_3 aerosols play a critical role in the destruction of stratospheric ozone over Antarctica during the Austral Spring (Solomon and Schoeberl, 1988), has led to similar questions concerning the possibility that H_2SO_4 aerosols, of volcanic origin, may also catalyze the destruction of ozone in the mid-latitudes. Thus, at a time when the scientific questions become even more important, the conventional stratospheric ozone lidar (and many other passive instruments which depend on scattering of solar radiation) cannot retrieve an ozone profile in the critical region.

This paper describes and presents data from a lidar system which used Raman scattering from N_2 to provide the backscattered signal from regions which have volcanic aerosol present. These returns are shifted 2331 cm^{-1} from the transmitted wavelengths and the returns depend only upon the molecular density. There is no component in the backscattered return due to scattering from aerosols. Signals returned are strong enough to permit a continuous profile from 15 to 50 km using both the Raman and Rayleigh techniques.

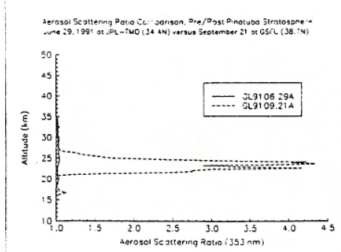

Figure 1: A plot of the Aerosol Backscatter Ratio for 6/29/91, prior to the arrival of the Mt. Pinatubo aerosol cloud, and for 9/21/91 after the cloud has dispersed as high as GSFC. Aerosol backscatter ratio = (Rayleigh + Mie)/Rayleigh.

[1]NASA/Goddard Space Flight Center, Laboratory for Atmospheres
[2]Hughes/STX Corporation

Paper number 93GL00751
0094-8534/93/93GL-00751$03.00

Raman lidar system for the measurement of water vapor and aerosols in the Earth's atmosphere

D. N. Whiteman, S. H. Melfi, and R. A. Ferrare

A nighttime operating Raman lidar system that is designed for the measurement of high ve... temporal resolution profiles of the water vapor mixing ratio and the aerosol backscattering... described. The theory of the measurements is presented. Particular attention is given to op... problems that have been solved during the development of the system. Data are presented fr... 1987 and described in their meteorological context.

Key words: Raman, lidar, water vapor, aerosols.

I. Introduction

Water vapor and aerosols are two interesting atmospheric parameters that are accessible to remove measurement. The water vapor mixing ratio, which is defined as the mass of water vapor divided by the mass of dry air in a given volume, is conserved in atmospheric processes that do not involve evaporation or condensation. Thus the mixing ratio is useful as a tracer of air parcels and in understanding energy transport within the atmosphere. Increased knowledge of water vapor concentration and motion can lead to a better understanding of cloud formation, convective storm development, and the hydrological cycle. Aerosol measurements, on the other hand, are important in a number of research areas, such as the retrieval of atmospheric and surface characteristics from satellite data and the impact of aerosols on climate and air pollution studies.

Lidar is a well-established technique for measuring both water vapor and aerosols. The early work of Cooney[1] and Melfi *et al.*,[2] in the late 1960's demonstrated the technique of Raman spectroscopy in the measurement of tropospheric water vapor. Later Pourney *et al.*[3] demonstrated the possibility of producing imagery that depicts the temporal evolution of the water vapor mixing ratio profile. In 1985 Melfi and Whiteman[4] extended this capability in both ... and temporal resolution. Vaughan *et al.*[5] have taken mixing ratio measurements up t... tropopause, and Melfi *et al.*[6] have used Raman li... record the passage of frontal systems. These mea... ments have demonstrated that Raman lidar c... used as a meteorological research tool that is u... in its ability to capture the spatial and tem... evolution of water vapor in the lower atmospher... the other hand, aerosol measurements were the... application of lidar in the early 1960's. For exa... the semipermanent stratospheric aerosol layer... was first measured by Junge and Manson[7] by u... balloons was later measured by using lidar.[8] ... recently the measurement of aerosol concentra... has been used to discern cloud top heights[9] and... height of the boundary layer and its variation.[10]

This paper describes a Raman lidar system th... capable of measuring both the water vapor mi... ratio and the aerosol backscattering ratio with s... cient reliability to allow essentially continuous ni... time operation. The method that is employed in... measurements is described, and the theory is ... cussed next. The equipment is then detailed. Emp... sis is given to the solutions of several operatio... problems that can limit lidar measurements of t... kind. The various methods of analysis are th... discussed, and the results are presented from rec... intensive measurement programs that were co... ducted in Greenbelt, Md., on Cape Cod, Mass., and Wallops Island, Va.

II. Method

The experiment is based on a frequency-tripled N... YAG laser transmitter, an optical telescope receive...

D. N. Whiteman is with the Laboratory for Terrestrial Physics, NASA Goddard Space Flight Center, Code 924, Greenbelt, Maryland 20771. S. H. Melfi and R. A. Ferrare are with the Laboratory for Atmospheres, NASA Goddard Space Flight Center, Code 917, Greenbelt, Maryland 20771. R. A. Ferrare is also with the Universities Space Research Association.

Received 29 May 1990.
0003-6935/92/163068-15$05.00/0.

Differential absorption and Raman lidar for water vapor profile measurements: a review

William B. Grant, MEMBER SPIE
NASA/Langley Research Center
Atmospheric Sciences Division
MS 401A
Hampton, Virginia 23665-5225

Abstract. Differential absorption lidar and Raman lidar have been applied to the range-resolved measurements of water vapor density for more than 20 years. During this period, there have been considerable advances in laser and lidar technology, as well as in the understanding of the factors required to optimize both lidar techniques for water vapor measurements. Results have been obtained using both lidar techniques that have led to improved understanding of water vapor distributions in the atmosphere. This paper reviews the theory of the measurements, including the sources of systematic and random error; the progress in lidar technology and techniques during that period, including a brief look at some of the lidar systems in development or proposed; and the steps being taken to improve such lidar systems.

Subject terms: lidar; Raman lidar; differential absorption lidar; water vapor; Raman scattering; dye laser; alexandrite laser; Ti:Al_2O_3 laser.

Optical Engineering 30(1), 40-48 (January 1991).

CONTENTS

1. INTRODUCTION

Water vapor is an important molecular species in the Earth's atmosphere that is highly variable in both time and space. It plays an important role in many atmospheric processes, such as weather, climate, and atmospheric photochemistry. Because its distribution in the atmosphere is highly variable, it is necessary to understand its spatial and temporal variability and to relate this to various atmospheric effects. Lidar, with its ability to provide range-resolved profiles in a short time (seconds or minutes), can be used to make unique remote measurements of water vapor distributions. Indeed, a number of lidar systems have been developed and demonstrated for water vapor measurements using either the differential absorption lidar (DIAL) technique[1–19] or the Raman scattering approach.[20–41] It is the purpose of this paper to review the history of applying both approaches to range-resolved measurements of water vapor, examine the advantages and limitations to the use of both techniques in various spectral regions, and outline the directions in which developments of these approaches are proceeding.

2. DIAL TECHNIQUE

The DIAL technique generally uses two laser wavelengths to determine the range-resolved profile of atmospheric trace molecular species.[42–45] Elastic backscatter from molecules (Rayleigh) and aerosols (Mie) provides the lidar signals. Molecular absorption along the path attenuates the lidar signal in a manner that can be used to determine the range-resolved profile of the species. One wavelength is tuned to an absorption feature of the molecular species of interest while the other is tuned off the absorption feature in a nearby region that is weakly or not absorbed by the species of interest. The lidar return from the "off" laser wavelength provides a reference signal for the atmospheric scattering from molecules and aerosols and for the slowly varying "background" atmospheric absorption that is common to both lidar wavelengths. The general expression for the power detected by the lidar system at the transmitted wavelength is

$$P(r) = \frac{Pc\tau AO(r)\eta b(r)\exp\left\{-2\int_0^r [an(r) + k(r)]dr\right\}}{2r^2} + B , \quad (1)$$

where $P(r)$ is the received power from range r (W), P is the transmitted power (W), c is the speed of light (3×10^8 m/s), τ is the pulse width of the laser beam (s), A is the receiver area (m^2), $O(r)$ is the transmitter/receiver overlap function, r is the range to the region (m), η is the receiver/detector efficiency, $b(r)$ is the atmospheric backscatter coefficient ($m^{-1}\cdot sr^{-1}$), a is the absorption cross section of the molecular species of interest ($m^2\cdot molecule^{-1}$), $n(r)$ is the density of the molecular species of interest (m^{-3}), $k(r)$ is the total atmospheric extinction coefficient that does not include absorption due to the molecular species of interest (m^{-1}), and B is the detected background radiation level (W).

Once a suitable signal has been recorded at both wavelengths, which generally requires some signal averaging,[46] the ratio of the signals at the two laser wavelengths can be used with the

Paper LI-108 received June 15, 1990; revised manuscript received Sept. 11, 1990; accepted for publication Sept. 20, 1990.

Raman … the Pi…
standar… …stic D…

Independent measurement of extinction and backscatter profiles in cirrus clouds by using a combined Raman elastic-backscatter lidar

Albert Ansmann, Ulla Wandinger, Maren Riebesell, Claus Weitkamp, and Walfried Michaelis

Height profiles of the extinction and the backscatter coefficients in cirrus clouds are determined independently from elastic- and inelastic- (Raman) backscatter signals. An extended error analysis is given. Examples covering the measured range of extinction-to-backscatter ratios (lidar ratios) in ice clouds are presented. Lidar ratios between 5 and 15 sr are usually found. A strong variation between 2 and 20 sr can be observed within one cloud profile. Particle extinction coefficients determined from inelastic-backscatter signals and from elastic-backscatter signals by using the Klett method are compared. The Klett solution of the extinction profile can be highly erroneous if the lidar ratio varies along the measuring range. On the other hand, simple backscatter lidars can provide reliable information about the cloud optical depth and the mean cloud lidar ratio.

Key words: Combined lidar, Raman lidar, backscatter lidar, lidar ratio, particle extinction, particle backscatter, Klett method, cirrus observation.

1. Introduction

High-altitude cirrus clouds have been identified as one important regulator of the radiance balance of the earth-atmosphere system.[1] In particular, optically thin cirrus are of great interest since an increase of the area covered by these clouds, which may be induced partly by contrails, is expected to enhance the greenhouse effect. In spite of the importance of ice clouds, measurements of their microphysical properties (ice-crystal characteristics) and of their radiative properties (extinction, reflection, and emission) are rare[1] mainly because of their high location in the atmosphere. Extended studies of cirrus clouds were performed only recently in two regional experiments, the First International Satellite Cloud Climatology Project (ISCCP) Regional Experiment (FIRE)[2] and the International Cirrus Experiment (ICE).[3] In both investigations high-flying aircraft as well as ground-based observation stations were utilized.

In this paper, lidar measurements taken in cirrus clouds during ICE'89 in September and October 1989 are presented. For what is, to our knowledge, the first time, profiles of the extinction and backscatter coefficients in high-level ice clouds are measured independently of each other with a combined Raman elastic-backscatter lidar. In the technique applied, short laser pulses at a wavelength of 308 nm are transmitted vertically into the atmosphere, and the height profiles of signals elastically backscattered by air molecules and particles (at 308 nm) and inelastically (Raman) backscattered by nitrogen molecules at 332 nm (vibrational-rotational spectrum) are recorded. The particle extinction coefficient is determined from the inelastic-backscatter signal profile,[4] while the particle backscatter coefficient is derived from the ratio of the elastic backscatter to the Raman signal, as is usual in the combined lidar technique.[5,6]

The independent measurement of the particle extinction and backscatter coefficients and, thus, of the extinction-to-backscatter ratio, or lidar ratio, provides information on the transmission and the reflection properties of cirrus clouds and also on the ice-crystal characteristics because the lidar ratio depends on shape, size, and orientation of the anisotropic ice particles. The influence of the microphysical properties on the extinction-to-backscatter ratio is discussed here on the basis of measurement examples.

The lidar ratio is one important input parameter

The authors are with the Institut für Physik, GKSS-Forschungszentrum Geesthacht GmbH, Postfach 1160, W-2054 Geesthacht, Germany.

Received 5 June 1991.
0003-6935/92/337113-19$05.00/0.

Appl. Phys. B 55, 18–28 (1992)

Applied Physics B Photo-physics and Laser Chemistry

Combined Raman Elastic-Backscatter LIDAR for Vertical Profiling of Moisture, Aerosol Extinction, Backscatter, and LIDAR Ratio

A. Ansmann, M. Riebesell, U. Wandinger, C. Weitkamp, E. Voss, W. Lahmann, and W. Michaelis

GKSS-Forschungszentrum Geesthacht GmbH, Postfach 1160, W-2054 Geesthacht, Fed. Rep. Germany

Received 18 November 1991/Accepted 13 February 1992

Abstract. A combined Raman elastic-backscatter lidar has been developed. A XeCl excimer laser is used as the radiation source. Inelastic Raman backscatter signals are spectrally separated from the elastic signal with a filter or grating polychromator. Raman channels can be chosen to register signals from CO_2, O_2, N_2, and H_2O. Algorithms for the calculation of the water-vapor mixing ratio from the Raman signals and the particle extinction and backscatter coefficients from both elastic and inelastic backscatter signals are given. Nighttime measurements of the vertical humidity distribution up to the tropopause and of particle extinction, backscatter, and lidar ratio profiles in the boundary layer, in high-altitude water and ice clouds, and in the stratospheric aerosol layer are presented. Daytime boundary-layer measurements of moisture and particle extinction are made possible by the improved daylight suppression of the grating polychromator. Test measurements of the CO_2 mixing ratio indicate the problems for the Raman lidar technique in monitoring other trace gases than water vapor.

PACS: 42.68.Rp, 93.85.+q, 94.10.Gb, 92.60.Jq

The measurement of tropospheric vertical water vapor distributions and of geometric (height, depth) and radiometric (extinction, backscattering) properties of aerosol and cloud layers with high spatial and temporal resolution is a basic requirement for the improved understanding of weather and climate, especially of the radiation and heat budget of the earth's atmosphere, and of atmospheric chemistry. Passive measurement techniques cannot adequately meet these requirements. In-situ measurements from airplanes or balloons are very costly and cannot provide data at low and high altitudes simultaneously. The latter shortcoming also applies to measurements with radiosondes. Passive methods using radiation from the sun (or moon) lack the required height resolution. Ground-based, height-resolving, simultaneously measuring devices have therefore been developed. High-resolution water vapor profiles can be obtained from lidar measurements using both the Raman [1–9] or the differential absorption lidar (DIAL) technique [10–18]. Lidars are also powerful tools for the detection of aerosol and cloud layers and for the determination of their geometric and backscattering properties. In addition to these data, a combined Raman elastic-backscatter lidar allows the simultaneous and independent measurement of height profiles of the particle extinction and backscatter coefficients. The resulting extinction-to-backscatter, or lidar, ratio reveals several microphysical properties of aerosol or cloud layers because backscattering and extinction depend in different ways on the size, shape etc. of the scattering particles. The lidar ratio cannot be derived from the data of simple backscatter lidars, but is needed to allow an estimation of the particle optical depth from the elastic-backscatter return signal profile [19–21].

The primary data collected with the combined Raman elastic-backscatter lidar are the height profiles of the Raman-scattered radiation from the molecules of nitrogen or oxygen and of water vapor, and of the elastically backscattered radiation from both air molecules and aerosol particles. A xenon chloride excimer laser emitting at a wavelength of 308 nm is used as the radiation source. For separation of the different backscatter lines two specially designed polychromators of the interference filter and of the grating type are available. At nighttime, in the absence of strong daylight background, the interference filter polychromator is normally used for the detection of the very weak Raman backscatter intensities because of its higher transmission in the different channels. The grating polychromator has smaller spectral bandwidth. It therefore allows the determination of water-vapor mixing-ratio profiles in the boundary layer at daytime. This device

AtmoHead 2024 – 15-17 July 2024 – Ischia - Italy

$$L_E(s) = L(s) \cdot [\beta_{mol}(s,\pi) + \beta_{aer}(s,\pi)] \cdot \Delta s \cdot \frac{A_E}{s^2} \cdot T_{aer}(s) \cdot T_{mol}(s) \cdot G_E(s).$$

Elastic lidar EQ

$$L(s) = L_o \cdot T_{aer}(s) \cdot T_{mol}(s)$$

$$T_{aer}(s) = exp\left(-\int_0^s \alpha_{aer}(s')ds'\right),$$

$$T_{mol}(s) = exp\left(-\int_0^s \alpha_{mol}(s')ds'\right),$$

$$L_E(s) = L(s) \cdot [\beta_{mol}(s,\pi) + \beta_{aer}(s,\pi)] \cdot \Delta s \cdot \frac{A_E}{s^2} \cdot T_{aer}(s) \cdot T_{mol}(s) \cdot G_E(s).$$

Elastic lidar EQ

$$\eta_{to}^{\lambda_o} \eta_{ro}^{\lambda_0} \eta_{re}^{\lambda_0} A = A_E$$

$$L(s) = L_o \cdot T_{aer}(s) \cdot T_{mol}(s)$$

$$T_{aer}(s) = exp\left(-\int_0^s \alpha_{aer}(s')ds'\right),$$

$$T_{mol}(s) = exp\left(-\int_0^s \alpha_{mol}(s')ds'\right),$$

The expected photon counts $L_E(s)$ are proportional to the product of the

(1) transmitted laser photon number,

(2) probability that a transmitted photon is scattered,

(3) probability that a scattered photon is collected (acceptance solid angle) $\frac{A}{s^2}$

(4) light transmission through medium, and

(5) overall system efficiency. $\eta_{to}^{\lambda_o} \eta_{ro}^{\lambda_0} \eta_{re}^{\lambda_0}$

Background photon counts and detector noise also contribute to the expected photon counts: $L_{E+b}(s) = L_E(s)$+bkg (which must be considered in error analysis)

$$L_E(s) = L(s) \cdot [\beta_{mol}(s,\pi) + \beta_{aer}(s,\pi)] \cdot \Delta s \cdot \frac{A_E}{s^2} \cdot T_{aer}(s) \cdot T_{mol}(s) \cdot G_E(s).$$

Elastic lidar EQ

$$L(s) = L_o \cdot T_{aer}(s) \cdot T_{mol}(s)$$

$$T_{aer}(s) = exp\left(-\int_0^s \alpha_{aer}(s')ds'\right),$$

$$T_{mol}(s) = exp\left(-\int_0^s \alpha_{mol}(s')ds'\right),$$

Elastic lidar inversion

$$L_E(s) = L(s)\cdot[\beta_{mol}(s,\pi)+\beta_{aer}(s,\pi)]\cdot\Delta s\cdot\frac{A_E}{s^2}\cdot T_{aer}(s)\cdot T_{mol}(s)\cdot G_E(s).$$

$$[\beta_{mol}(s,\pi)+\beta_{aer}(s,\pi)] = \frac{L_E(s)\cdot s^2}{K_E\cdot T^2_{mol}(s)}\cdot T^{-2}_{aer}(s)$$

$$K_E = \frac{L_E(s_0)\cdot {s_0}^2}{[\beta_{mol}(s_0,\pi)+\beta_{aer}(s_0,\pi)]\cdot T^2_{mol}(s_0)}\cdot T^{-2}_{aer}(s_0)$$

$$\alpha_{aer}(s) = \mathrm{LR}\cdot\beta_{aer}(s,\pi)$$

hypotesis

Step 0:

$$K_E = \frac{L_E(s_0)\cdot {s_0}^2}{[\beta_{mol}(s_0,\pi)+\beta_{aer}(s_0,\pi)]\cdot T^2_{mol}(s_0)} \leftarrow T^{-2}_{aer}(s_0) = 1$$

$$[\beta_{mol}(s,\pi)+\beta_{aer}(s,\pi)] = \frac{L_E(s)\cdot s^2}{K_E\cdot T^2_{mol}(s)}$$

Step 1:

$$T_{aer}(s) = exp\left(-\int_0^s \alpha_{aer}(s')ds'\right)$$

$$= exp\left(-\mathrm{LR}\int_0^s \beta_{aer}(s',\pi)ds'\right)$$

$$K_E = \frac{L_E(s_0)\cdot {s_0}^2}{[\beta_{mol}(s_0,\pi)+\beta_{aer}(s_0,\pi)]\cdot T^2_{mol}(s_0)}\cdot T^{-2}_{aer}(s_0)$$

$$[\beta_{mol}(s,\pi)+\beta_{aer}(s,\pi)] = \frac{L_E(s)\cdot s^2}{K_E\cdot T^2_{mol}(s)}\cdot T^{-2}_{aer}(s)$$

Lidar equation contains two unknown sets of parameters: aerosol extinction and aerosol backscatter.
Equation can only be solved with prescribed lidar ratio (extinction to backscatter ratio).
The validity of the assumption of a constant particulate lidar ratio depends on the actual atmospheric conditions.
The lidar ratio depends on the type, shape, composition, and size distribution of the atmospheric particulates.
If these parameters do not significantly change along the examined path, this assumption is reasonable, even if these parameters vary slightly because of small-scale fluctuations… **but is not always the case.**
The lidar ratio assumption and hence the not independent retrieval of the aerosol backscatter and extinction made necessary the development of the **Raman Lidar**

Mattis at al., Atmos. Meas. Tech., 9, 3009–3029, 2016

Until convergence i.e.
$\Delta K_E/K_E < 0.01$ or better.

Raman lidar EQ (N_2)

$$L_R(s) = L(s) \cdot \left[\beta^R_{N_2}(s,\pi)\right] \cdot \Delta s \cdot \frac{A_R}{s^2} \cdot T^R_{aer}(s) \cdot T^R_{mol}(s) \cdot G_R(s).$$

Raman lidar EQ (H_2O)

$$L_H(s) = L(s) \cdot \left[\beta^R_{H_2O}(s,\pi)\right] \cdot \Delta s \cdot \frac{A_H}{s^2} \cdot T^H_{aer}(s) \cdot T^H_{mol}(s) \cdot G_R(s).$$

$L_R(s$

$= L($

$\cdot T^R_{mo}$

Raman aerosol lidar

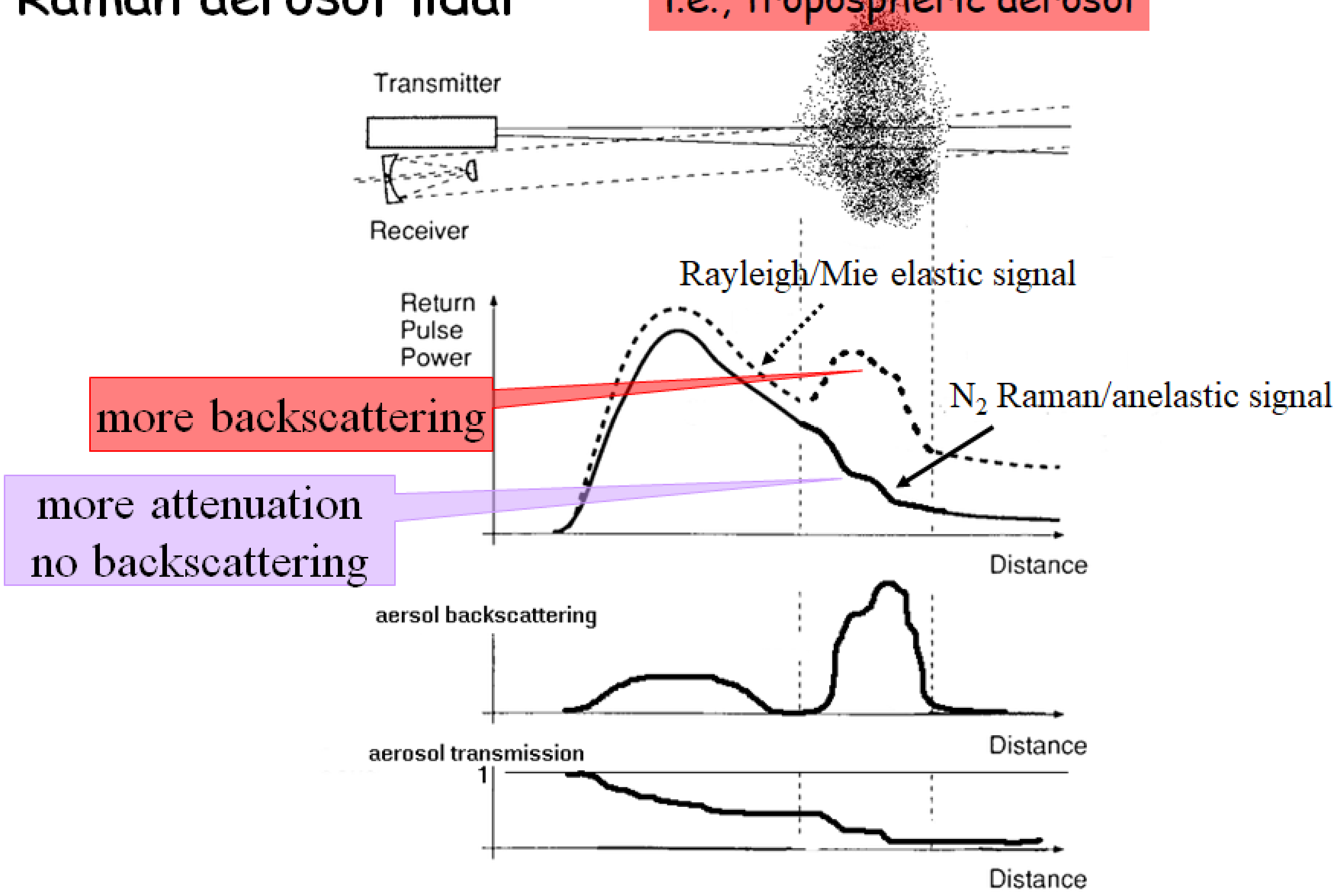

(s)

$L_R(s)$

$= L(s)$

$\cdot T^R_{mol}($

Raman lidar EQ (N_2)

$^H_{aer}(s)$

[The Raman lidar technique] It's a robust technique makes low demands concerning spectral purity of the emitted laser light and frequency stabilization of the receiver. However, it suffers from the low cross sections of Raman scattering and thus from the comparably **small signal-to-noise ratios of the measurements**.

For a long time, Raman lidar instruments were therefore **mainly used at nighttime**. Daytime applications increased with the development of **high-power transmitters and narrow-bandwidth detection systems which allow a sufficient suppression of the daylight background.**

Ulla Wandinger "Raman Lidar" in "Lidar Range-Resolved Optical Remote Sensing of the Atmosphere" Springer 2005

Angstrom Exponent

$$\alpha_{aer}(s) = \frac{\frac{s^2 L_R(s)}{G_R(s) n_{mol}(s)} \cdot \frac{d}{ds}\left[\frac{G_R(s) n_{mol}(s)}{s^2 L_R(s)}\right] - \alpha_{mol}(s) - \alpha_{mol}^R(s)}{1 + \left(\frac{\lambda_o}{\lambda_R}\right)^{k}}$$

G. Pappalardo, A. Amodeo, M. Pandolfi, U. Wandinger, A. Ansmann, J. Bosenberg, V. Matthias, V. Amiridis, F. De Tomasi, M. Frioud, M. Iarlori, L. Komguem, A. Papayannis, F. Rocadenbosch e X. Wang, «Aerosol lidar intercomparison in the framework of the EARLINET project. 3. Raman lidar algorithm for aerosol extinction, backscatter, and lidar ratio,» Appl. Opt., vol. 43, p. 5370–5385, 2004.

Aerosol extinction (from N_2 signal)

$$\beta_{aer}(s,\pi) = \beta_{aer}(s) = \beta_{mol}(s) \cdot f_{N_2} \cdot \left[\frac{L_E(s)}{L_R(s)} \cdot \frac{A_E}{A_R} \cdot \frac{\frac{d\sigma_{N_2}^R(\pi)}{d\Omega}}{\frac{d\sigma_{mol}(s,\pi)}{d\Omega}} \cdot \frac{G_R(s)}{G_E(s)} \cdot \frac{T_{aer}^R(s) \cdot T_{mol}^R(s)}{T_{aer}(s) \cdot T_{mol}(s)} - 1\right]$$

Aerosol backscatter (from AIR & N_2 signal)

The constant C is determined by imposing that the AOD below the complete overlap is a linear function through the origin of the range.

$$\tau_{aer}(s) = -\frac{\log\left(\frac{C \cdot s^2 L_R(s)}{T_{mol}(s) \cdot T_{mol}^{R}(s) \cdot n_{mol}(s)}\right)}{1 + \left(\frac{\lambda_o}{\lambda_R}\right)^k}.$$

AOD
From N_2 signal

OR

$$\tau_{aer}(s_l, s) = \int_{s_l}^{s} \alpha_{aer}(s')ds'.$$

$$\tau_{aer}(s) = \alpha_{aer}(s_l) \cdot s_l + \tau_{aer}(s_l, s).$$

Water Vapor mixing ratio (g/kg) From H_2O & N_2 Raman signal

V. Rizi, M. Iarlori, G. Rocci e G. Visconti, «Raman lidar observations of cloud liquid water,» Applied Optics, vol. 43, n. 35, pp. 6440-6453, 2004.

$$\chi(s) = \boxed{C_{H20}} \cdot \frac{L_H(s)}{L_R(s)} \cdot \frac{T^R_{mol}(s)}{T^H_{mol}(s)} \cdot \frac{T^R_{mol}(s)}{T^H_{aer}(s)}$$

$$C_{\mathrm{H_2O}} = 0.7808 \frac{M_H}{M_{\mathrm{dryair}}} \frac{\frac{d\sigma_N(\pi)}{d\Omega}}{\frac{d\sigma_H(\pi)}{d\Omega}} K_{N,H}$$

$$\chi_{LIDAR} = \chi_{RAOB} \quad \Rightarrow \quad C_{\mathrm{H_2O}}$$

Can be determined with linear regression Y=AX

RAwinsonde OBservation (RAOB)

Aerosol backscatter (from AIR & N_2 signal)

Calibration procedure to find C_β

Mattis at al., Atmos. Meas. Tech., 9, 3009–3029, 2016

- (Usually) in a particle-free region in the free troposphere.
- A calibration window of width is shifted through the altitude region, where particle-free conditions typically occur.
- Foreach window position, the average and standard deviation of the signal or signal ratio is calculated.
- It is assumed that the window position where the signal or signal ratio has its minimum is closest to the assumed particle-free conditions.
- The average value within this calibration window and its standard deviation are used to estimate the calibration factor and its statistical uncertainty.
- If the ancillary data or from climatological data of the stratospheric particle load **it is possible to provide a BSR different from 1 as calibration value.**
- **This method has the disadvantage that it does not guarantee that there are no particles at all in the calibration window**. The algorithm would find a minimum also in the case that there are fewer particles than in other altitude regions only.
- **Stronger criterion to find particle free regions would be a test whether the measured signals have the same shape of a theoretically assumed Rayleigh signal (Baars et al. Atmos. Chem. Phys., 16, 5111–5137, 2016)**

$$\beta_{aer}(s,\pi) = \beta_{aer}(s)$$

$$= \beta_{mol}(s) \cdot f_{N_2} \cdot \left[\frac{L_E(s)}{L_R(s)} \cdot \frac{A_E}{A_R} \cdot \frac{\frac{d\sigma^R_{N_2}(\pi)}{d\Omega}}{\frac{d\sigma_{mol}(s,\pi)}{d\Omega}} \cdot \frac{G_R(s)}{G_E(s)} \cdot \frac{T^R_{aer}(s) \cdot T^R_{mol}(s)}{T_{aer}(s) \cdot T_{mol}(s)} - 1 \right]$$

$$= \beta_{mol}(s) \cdot [C_\beta \cdot UBSR(s) - 1]; \boldsymbol{C_\beta \cdot UBSR(s) = \frac{\beta_{aer}(s)}{\beta_{mol}(s)} + 1 = BSR(s)}$$

Calibration region where β_{aer}=0 (or other known value)

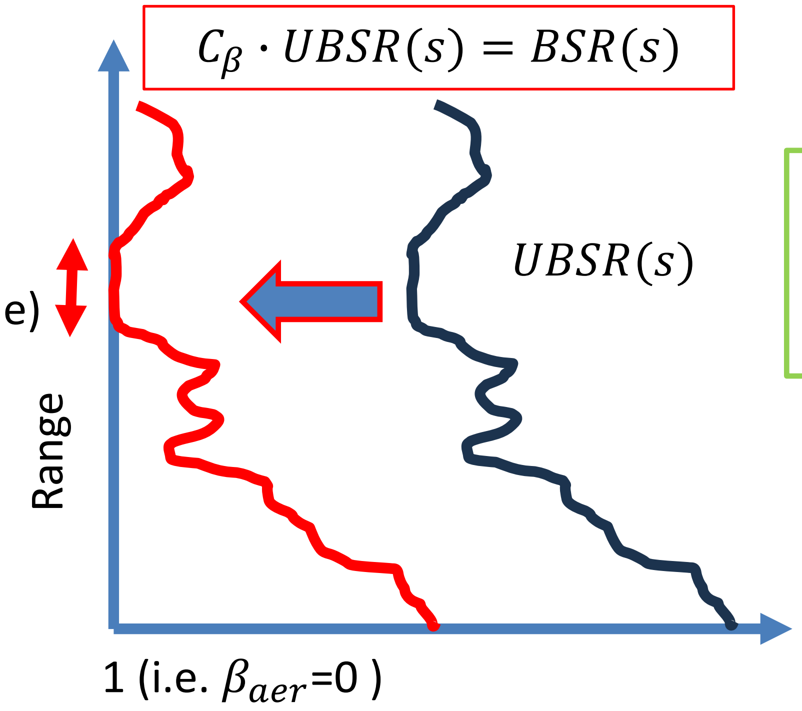

$$\frac{G_R(s)}{G_E(s)} \sim 1$$

But be careful…

$$\alpha_{aer}(s) = \frac{\frac{s^2 L_R(s)}{G_R(s) n_{mol}(s)} \cdot \boxed{\frac{d}{ds}\left[\frac{G_R(s) n_{mol}(s)}{s^2 L_R(s)}\right]} - \alpha_{mol}(s) - \alpha_{mol}^R(s)}{1 + \left(\frac{\lambda_o}{\lambda_R}\right)^k}$$

Aerosol extinction (from N_2 signal)

$$\beta_{aer}(s,\pi) = \beta_{aer}(s)$$
$$= \beta_{mol}(s) \cdot f_{N_2}$$
$$\cdot \left[\frac{L_E(s)}{L_R(s)} \cdot \frac{A_E}{A_R} \cdot \frac{\frac{d\sigma_{N_2}^R(\pi)}{d\Omega}}{\frac{d\sigma_{mol}(s,\pi)}{d\Omega}} \cdot \frac{G_R(s)}{G_E(s)} \cdot \frac{T_{aer}^R(s) \cdot T_{mol}^R(s)}{T_{aer}(s) \cdot T_{mol}(s)} - 1\right]$$

Aerosol backscatter (from AIR & N_2 signal)

Probably the most used algorithms to smooth or differentiate data involve some kind of sliding least-squares polynomial fitting.

$$Y(r)=\sum_{j=0}^{m} a_j r^j \Rightarrow \frac{d}{dr}[Y(r)]=\sum_{j=1}^{m} j a_j r^{j-1}, \text{ locally over k(r) points with k(r)} > m$$

Aerosol extinction (from N_2 signal)

Adopting this point of view is simple but could not be very efficient and **"…the digital filter approach and the concept of smoothing polynomials yield identical results…"** **(Steffen, *Circ. Syst. Signal Pr.,* vol. 5, pp. 187-210, 1986)**. For example, the digital filters based on smoothing polynomials are widely known as Savitzky – Golay filters (SG) and include both smoothers and differentiators.

Finite impulse response (FIR) filter have:

$$y(n)=\sum_{k=-N}^{N} h(k)x(n-k)$$

The above Eq. is a representation of the *non-causal* **Linear Time Invariant (LTI) Finite Impulse Response (FIR) digital filter**, whose **frequency response** is:

$$H(\omega)=\sum_{k=-N}^{N} h(k)e^{-j\omega k}$$

Iarlori M., Madonna F., Rizi V., Trickl T and Amodeo A., Effective resolution concepts for lidar observations, Atm. Meas. Tech., vol. 8, p. 5157–5176, 2015.

$$H^{(1)}(\omega) = j\omega = \omega e^{j\pi/2}, 0 \leq \omega \leq \pi;$$
$$\boxed{|H^{(1)}(\omega)| = \omega.}$$

Ideal Derivative:
A noise adding process

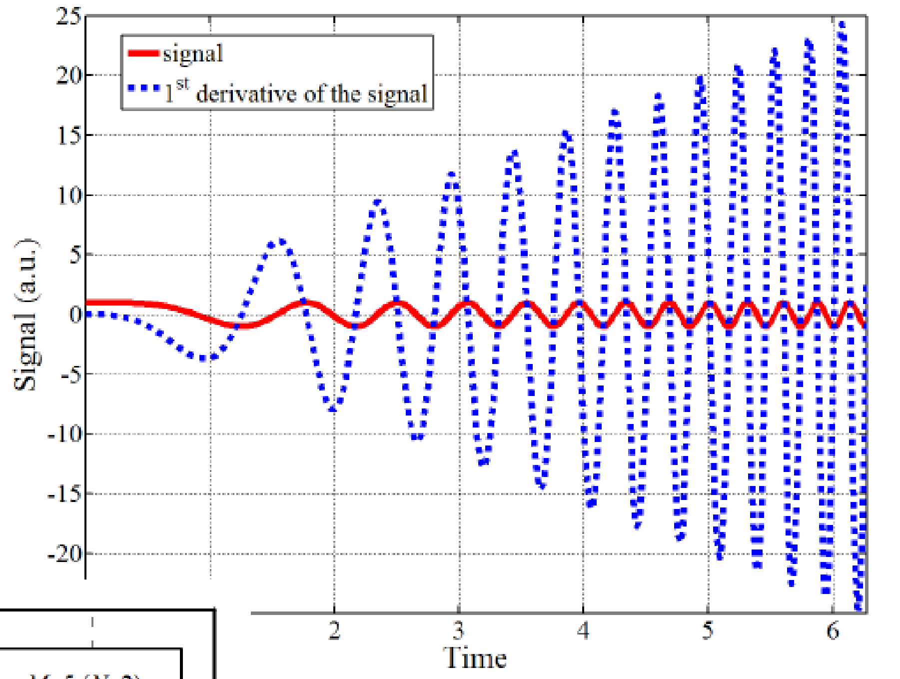

...the goal is to design a band-limited differentiator that, for frequencies higher than a certain cut-off value, will ideally remove the high-frequency component:

$$H^{(1)\mathrm{L}}(\omega) = H^{(1)}(\omega) H^{\mathrm{L}}(\omega).$$

$$\boxed{H^{(1)\mathrm{L}}(\omega) = -j \sum_{k=-N}^{N} h^{(1)\mathrm{L}}(k) \sin(\omega k)}$$

$$H^{\mathrm{L}}(\omega) = \frac{H^{(1)\mathrm{L}}(\omega)}{j\omega} = \frac{-\sum_{k=-N}^{N} h^{(1)\mathrm{L}}(k) \sin(\omega k)}{\omega}$$

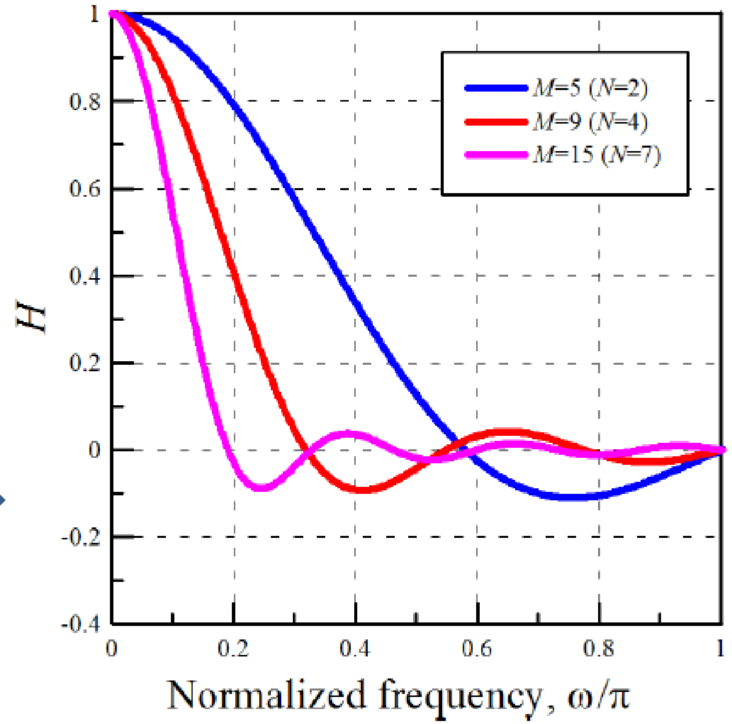

Aerosol extinction (from N_2 signal)

Iarlori M., Madonna F., Rizi V., Trickl T and Amodeo A., Effective resolution concepts for lidar observations, Atm. Meas. Tech., vol. 8, p. 5157–5176, 2015.

"**Epic failures: 11 infamous software bugs**" reports as the most likely reason of **the Mariner 1 space mission failure was caused by a not smoothed time derivative** of a radius:

...A more widely accepted account is that the punctuation mark was a superscript bar over a radius symbol, handwritten in a notebook. In rocket science, the overbar signifies a smoothing function, so the formula should have calculated the smoothed value of the time derivative of a radius. Without the smoothing function, even minor variations of the speed would trigger the corrective boosters to kick in. The automobile driving equivalent would be to yank the steering wheel in the opposite direction of every obstacle in the driver's field of vision.

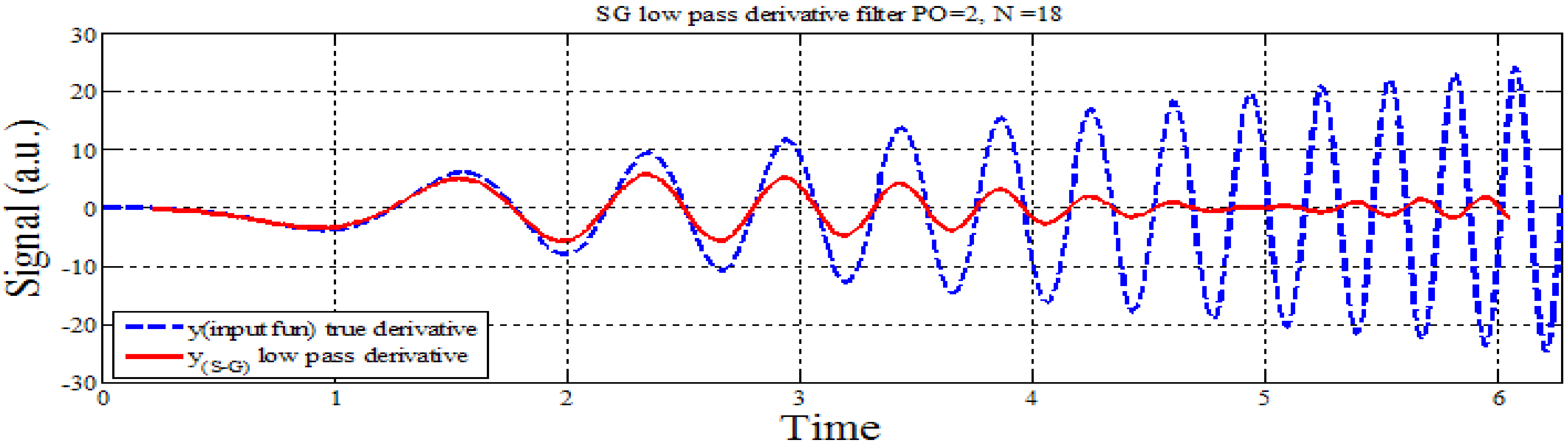

https://www.youtube.com/watch?v=0LJz-TWV3so

Derivative algorithm has a low pass digital filter embedded: **vertical resolution reduction because the removal of high frequency (small detail -> higher resolution). From Raw Resolution to Effective Resolution (ERes)**

$$\Delta R_{raw} \longrightarrow \Delta R_{eff}$$

Two approaches can be considered for the quantitative assessment of the ERes:

– The first one is related to the distortion induced by the smoothing process on any non-trivial input signal. In fact, the area preservation property (common to all the considered smoothing filters) implies that if the peak of a layer is reduced, its spatial width will increase and potentially could overlap with another feature present in a profile. The final result will be that it is no longer possible to distinguish one peak from another (i.e., they are no longer resolved): this means that a low-pass filter reduces the vertical resolution. This latter statement naturally leads to **the use of the Rayleigh criterion for the determination the effective resolution.**

– The second approach is based on the removal of high frequencies due to the smoothing operation : Noise Reduction Ratio (NRR) Criterion. Since high frequencies in space domain correspond to relatively small-scale details in the lidar profiles, if they are lost in a certain amount this will imply a reduction of the resolution in the output profile with respect to the input one. Incidentally, it should be noted that since a smoothing filter damps effectively only high frequencies and since it is common to deal with white noise, the low-frequency portion of the noise is still present in the smoothed signal, for example in the form of long-wave ripples.

Moreover, **a link is established between the ERes estimated with each of those two approaches and the corresponding cut-off frequency definition.**

Iarlori M., Madonna F., Rizi V., Trickl T and Amodeo A., Effective resolution concepts for lidar observations, Atm. Meas. Tech., vol. 8, p. 5157–5176, 2015.

Rayleigh Criterion

The Rayleigh criterion is a common metric for determining whether two points or lines are resolved. It states that the first zeros of two neighboring point or line spread functions overlap with the maximum of one over the first zero of the other.

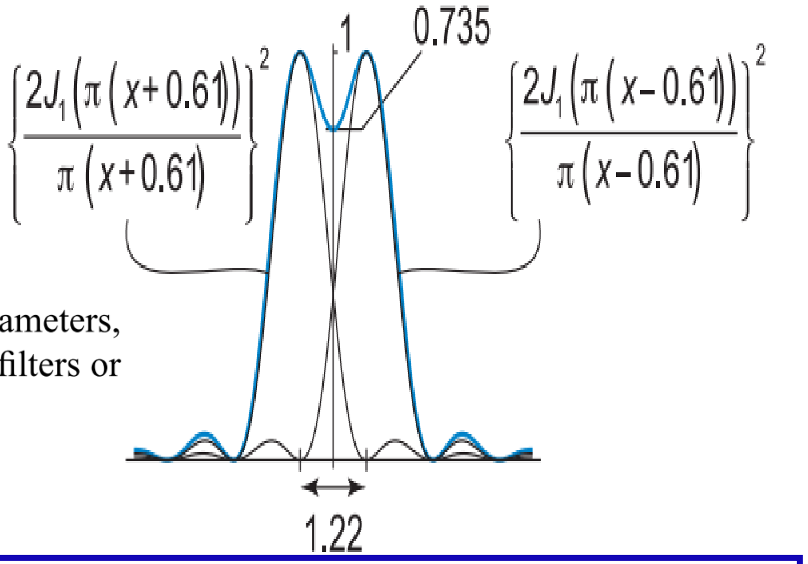

low-pass filter $L(\hat{p})$, characterized by a set of parameters, $\hat{p} = (p_1, p_2 \cdots, p_n)$ (e.g., $\hat{p} = (N, P)$ for SG-based filters or $\hat{p} = (\sigma)$ for a Gaussian filter)

$$\Delta R_{\mathrm{eff}}^{\mathrm{L}(\hat{p})}|_{\mathrm{Ray}} \approx \pi \frac{\Delta R_{\mathrm{raw}}}{\omega_{\mathrm{c}}^{\mathrm{L}(\hat{p})}|_{\mathrm{Ray}}} \approx \pi \frac{2\Delta R_{\mathrm{raw}}}{\omega_{\mathrm{sb}}^{\mathrm{L}(\hat{p})}}$$

The amount of zero-mean white noise removed by a generic low pass filter is:

$$\mathrm{NRR} = \frac{\mathrm{Var}_{\mathrm{OUT}}}{\mathrm{Var}_{\mathrm{IN}}} = \sum_{k=-N}^{N} [h(k)]^2$$

The ERes can be written by means of a general equation that depends only to the low-pass filter chosen:

$$\Delta R_{\mathrm{eff}}^{\mathrm{L}(\hat{p})}|_{\mathrm{NRR}} = \frac{\Delta R_{\mathrm{raw}}}{\mathrm{NRR}^{\mathrm{L}(\hat{p})}}$$

Iarlori M., Madonna F., Rizi V., Trickl T and Amodeo A., Effective resolution concepts for lidar observations, Atm. Meas. Tech., vol. 8, p. 5157–5176, 2015.

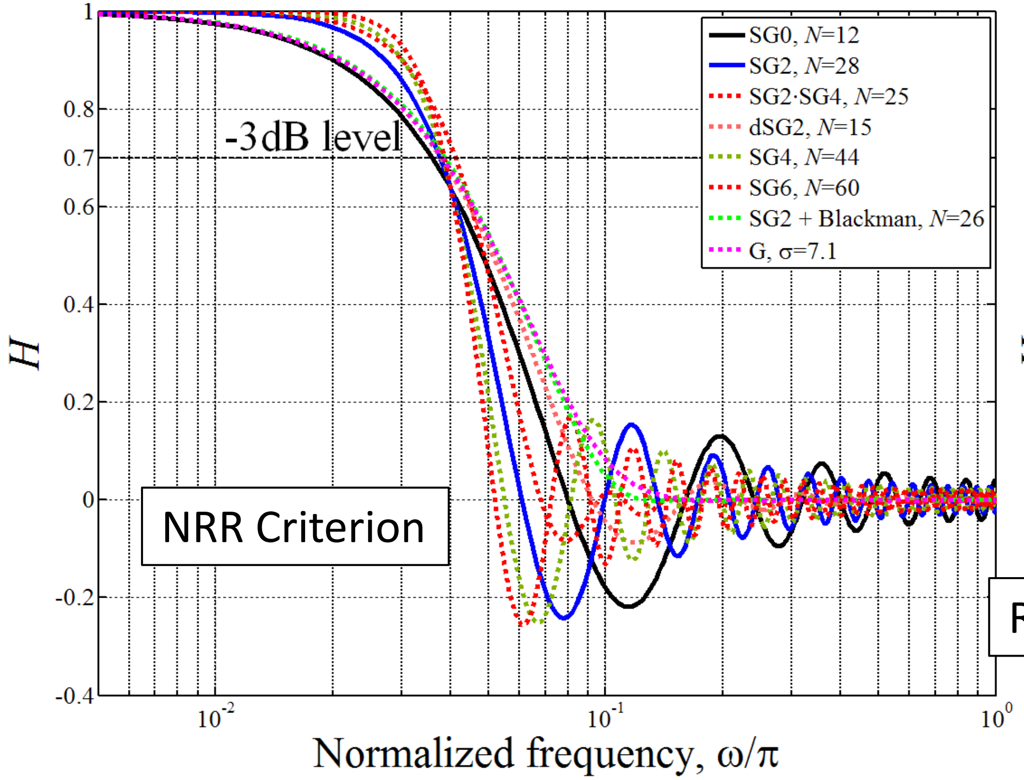

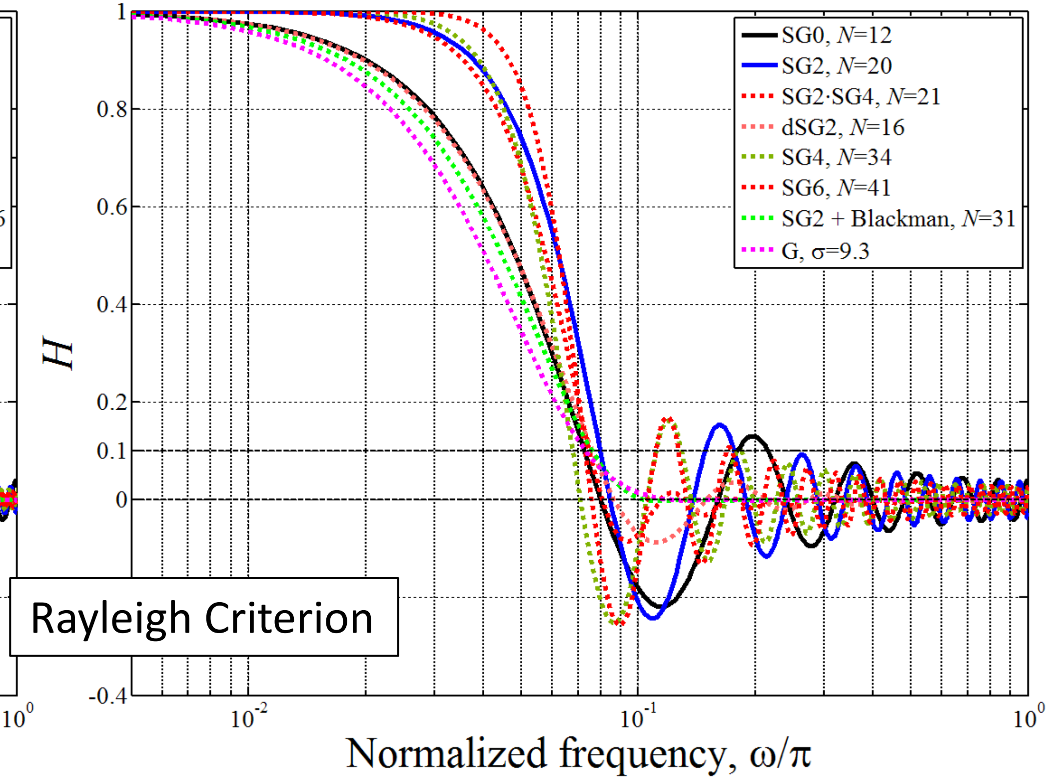

$$\begin{cases} \Delta R_{\text{eff}}^{\text{L}(\hat{p})}|_{\text{NRR}} \approx \pi \dfrac{\Delta R_{\text{raw}}}{\omega_{\text{c}}^{\text{L}(\hat{p})}|_{\text{NRR}}} \approx \pi \dfrac{\Delta R_{\text{raw}}}{\omega\left(H_{-3\text{dB}}^{\text{L}(\hat{p})}\right)}; \\ \Delta R_{\text{eff}}^{\text{L}(\hat{p})}|_{\text{Ray}} \approx \pi \dfrac{\Delta R_{\text{raw}}}{\omega_{\text{c}}^{\text{L}(\hat{p})}|_{\text{Ray}}} \approx \pi \dfrac{2\Delta R_{\text{raw}}}{\omega_{\text{sb}}^{\text{L}(\hat{p})}}. \end{cases}$$

– similar effective resolutions are obtained with the Rayleigh criterion for those filters that share a comparable stop band (ω_{sb}), irrespective of their behavior in the pass band;

– similar effective resolutions are obtained with the NRR criterion for different filters that have similar values in the −3dB cut-off frequency, $\omega|_{H_{-3\text{dB}}}$, i.e., a comparable pass band.

Iarlori M., Madonna F., Rizi V., Trickl T and Amodeo A., Effective resolution concepts for lidar observations, Atm. Meas. Tech., vol. 8, p. 5157–5176, 2015.

SG0 → Running mean

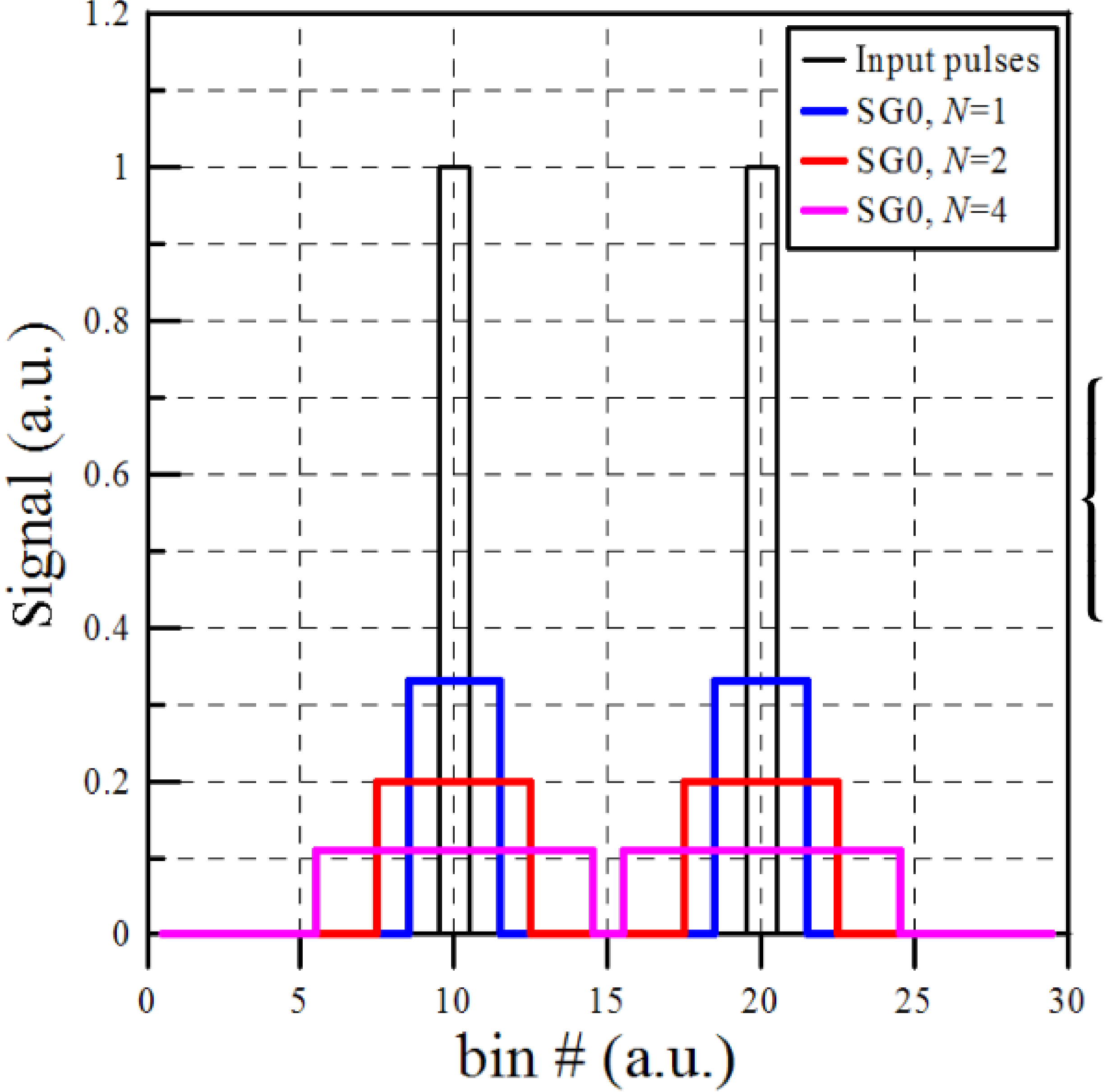

$$\boxed{\mathrm{NRR} = \frac{\mathrm{Var_{OUT}}}{\mathrm{Var_{IN}}} = \sum_{k=-N}^{N} [h(k)]^2}$$

$$\begin{cases} \mathrm{NRR}^{\mathrm{SG0(N)}} = \sum_{k=-N}^{N} \left[h^{\mathrm{SG0}}(k)\right]^2 = \dfrac{1}{2N+1}; \\ \Delta R_{\mathrm{eff}}^{\mathrm{SG0(N)}}\big|_{\mathrm{NRR}} = (2N+1)\Delta R_{\mathrm{raw}} = \dfrac{\Delta R_{\mathrm{raw}}}{\mathrm{NRR}^{\mathrm{SG0(N)}}}. \end{cases}$$

$$\boxed{\Delta R_{\mathrm{eff}}^{\mathrm{L}(\hat{p})}\big|_{\mathrm{NRR}} = \frac{\Delta R_{\mathrm{raw}}}{\mathrm{NRR}^{\mathrm{L}(\hat{p})}}}$$

Iarlori M., Madonna F., Rizi V., Trickl T and Amodeo A., Effective resolution concepts for lidar observations, Atm. Meas. Tech., vol. 8, p. 5157–5176, 2015.

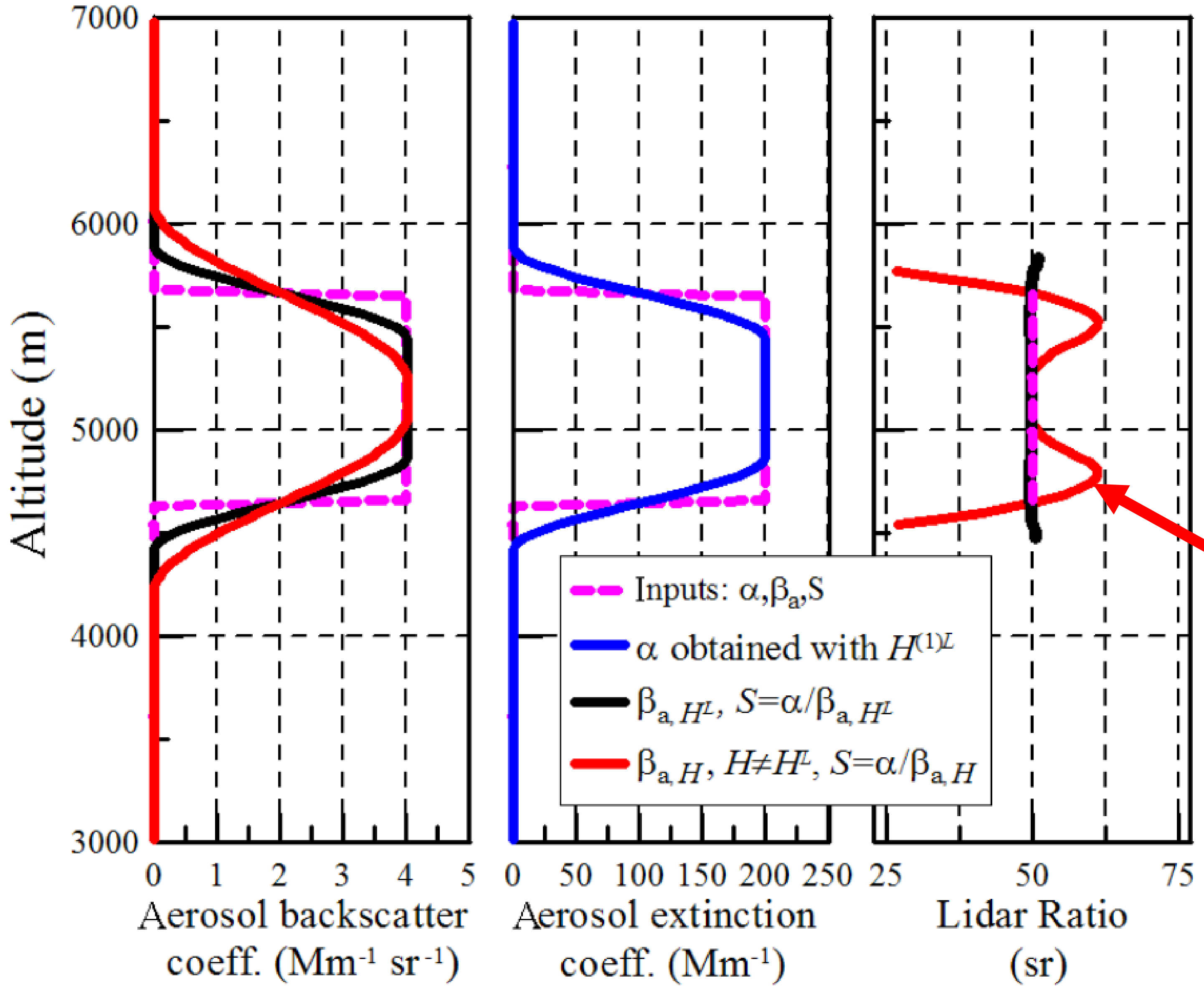

Lidar Ratio

Comparison have to be done between profiles with the same resolution otherwise…

…Wrong retrieval

Iarlori M., Madonna F., Rizi V., Trickl T and Amodeo A., Effective resolution concepts for lidar observations, Atm. Meas. Tech., vol. 8, p. 5157–5176, 2015.

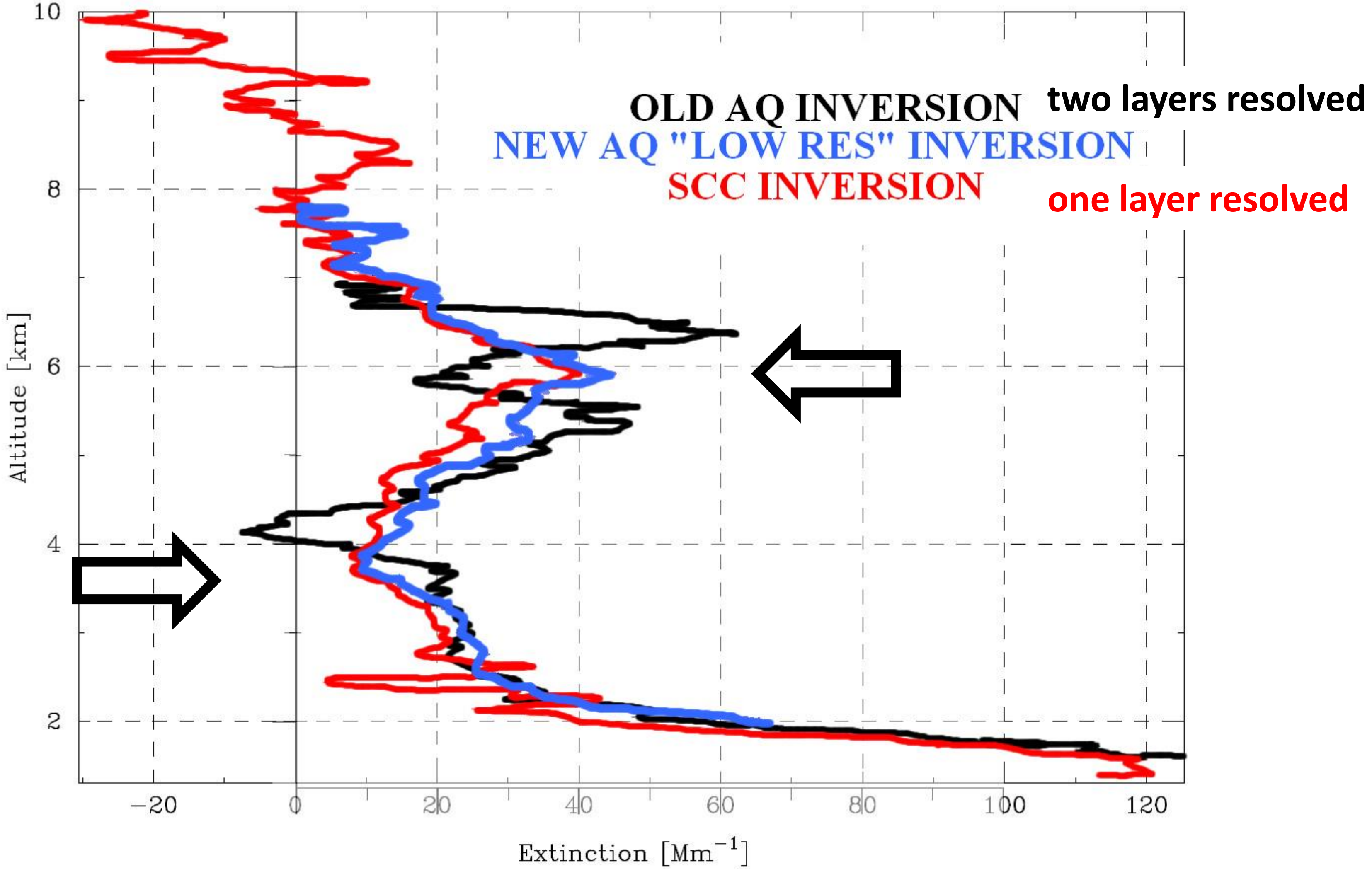

OLD AQ INVERSION
two layers resolved
NEW AQ "LOW RES" INVERSION
SCC INVERSION
one layer resolved
Altitude [km]
Extinction [Mm^{-1}]
10
8
6
4
2
−20
0
20
40
60
80
100
120

Same Effective resolution (750m)

-3dB level

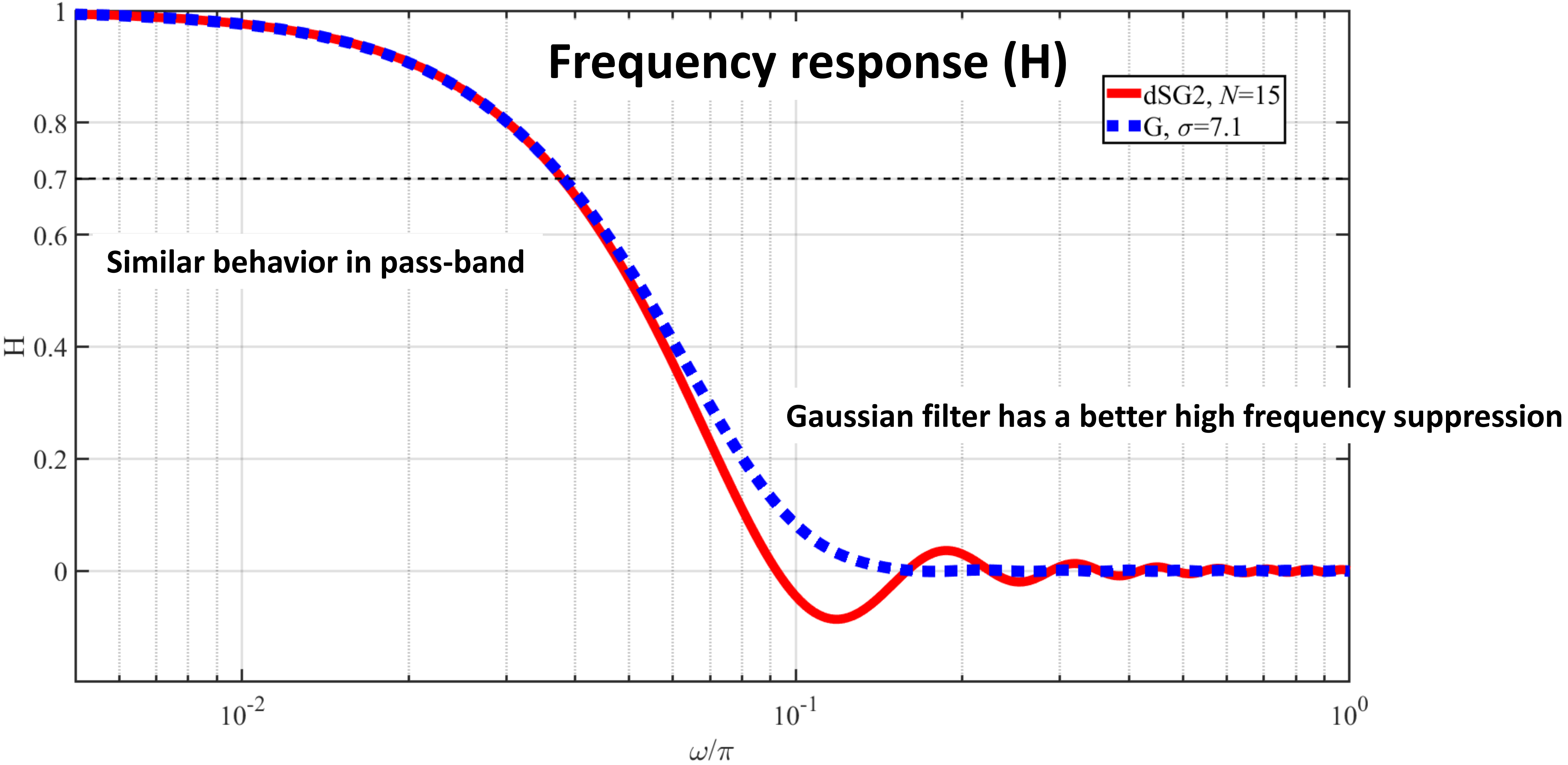

Smoothing Optimization

The smoothing of a signal could not always lead to significant improvement in the SNR (saturation effect when almost all the noise is removed).
For this reason, in a smoothing operation it seems relevant to find the limit over which the (undesirable) distortion of an underlying input signal could become more relevant than the concurrent (desirable) decrease of the noise level.

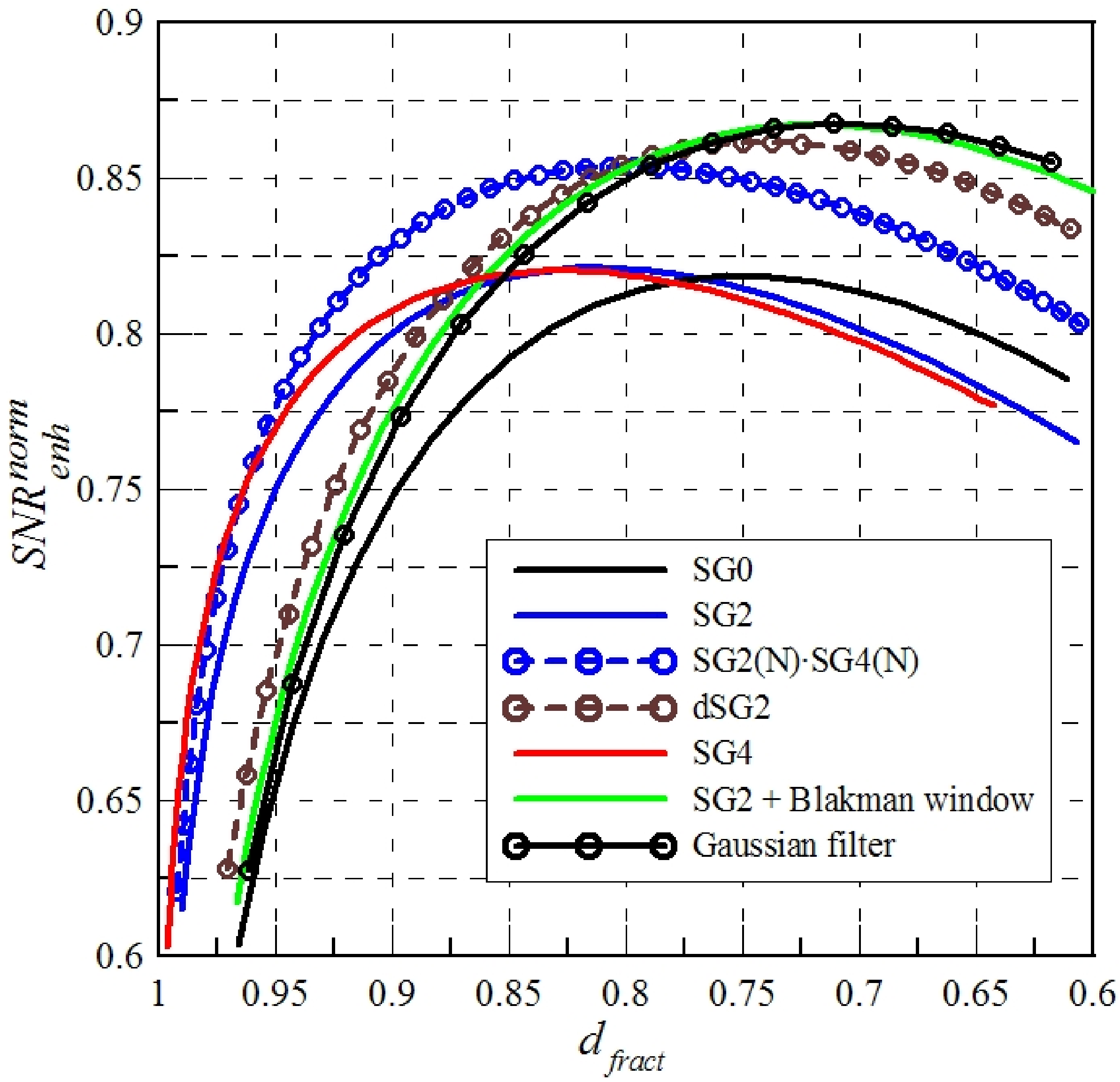

$$d_{fract} = \left(\frac{p_A}{p_B}\right);$$

p= peak value
σ=noise std
(B)efore and (A)fter smoothing

$$SNR_{enh} = \frac{SNR_A}{SNR_B} = \frac{\left(\frac{p_A}{\sigma_A}\right)}{\left(\frac{p_B}{\sigma_B}\right)} = \frac{d_{fract}}{\left(\frac{\sigma_A}{\sigma_B}\right)} \Rightarrow SNR_{enh}^{norm} = \frac{SNR_{enh}}{\sqrt{\frac{FWHM}{\Delta R_{raw}}}};$$

$$\frac{\sigma_A}{\sigma_B} = \sqrt{\sum_{k=-N}^{N}[h(k)]^2} = \sqrt{\mathrm{NRR}}$$

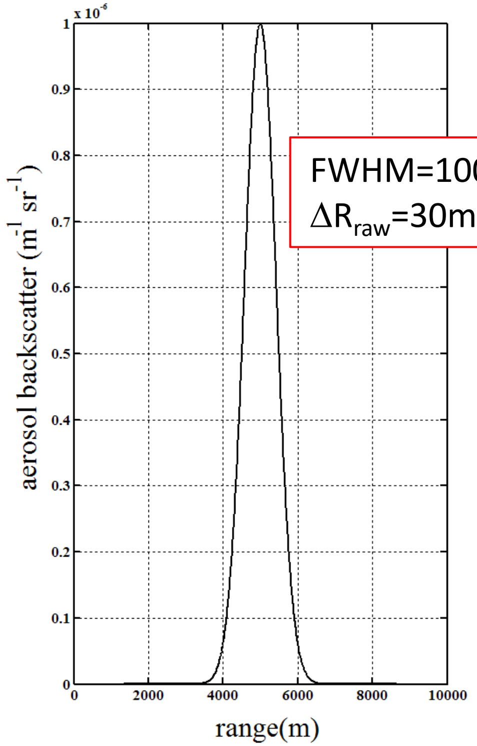

FWHM=1000m
ΔR_{raw}=30m

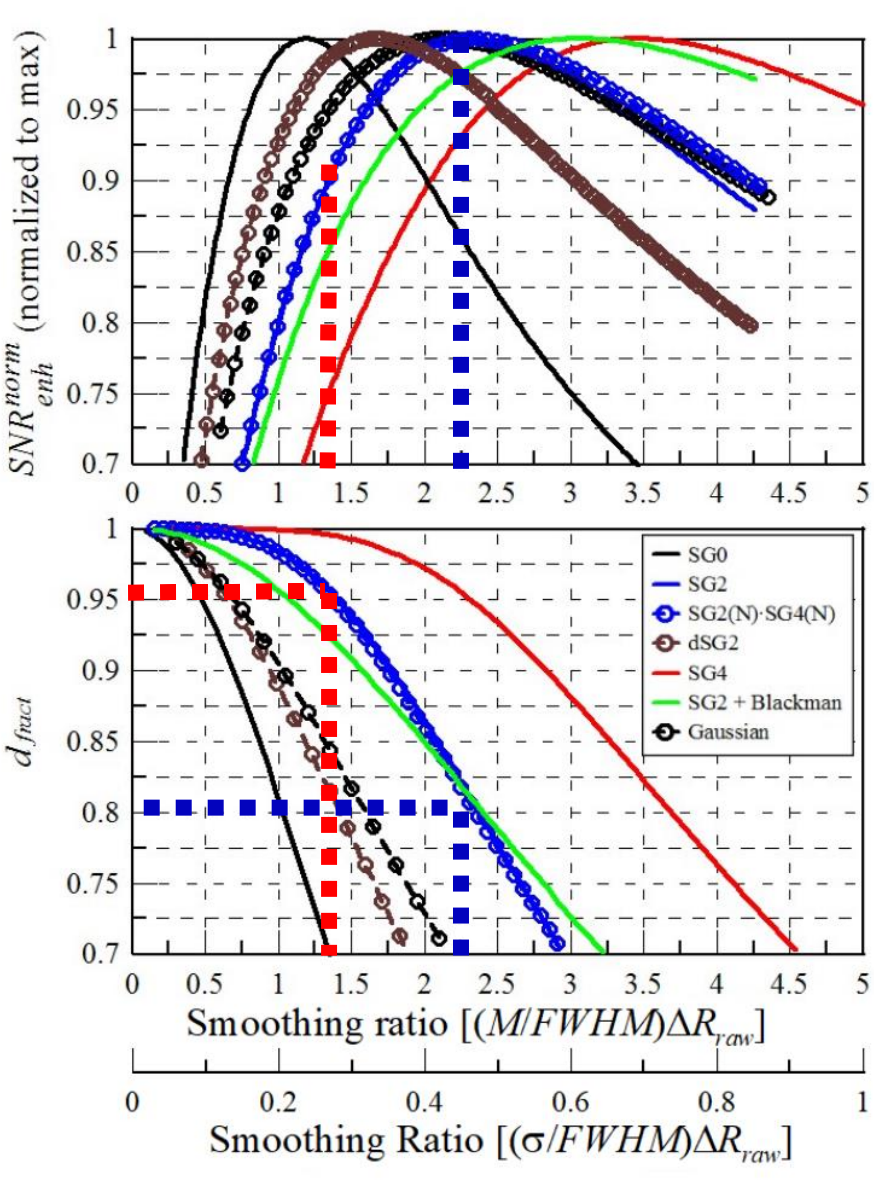

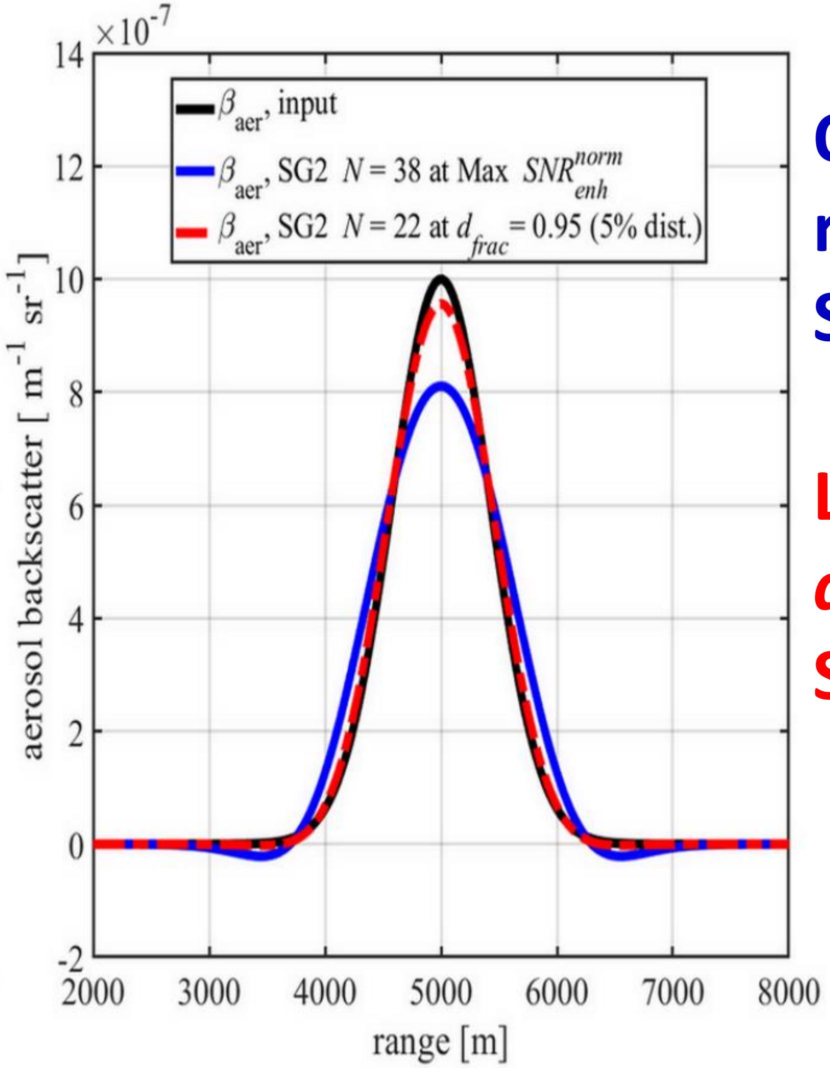

Optimization of Noise removal (SNR_{enh}^{norm}=1): SG2, N=38

Low distortion (es. 5% i.e. d_{fract}=0.95); SG2, N=22.

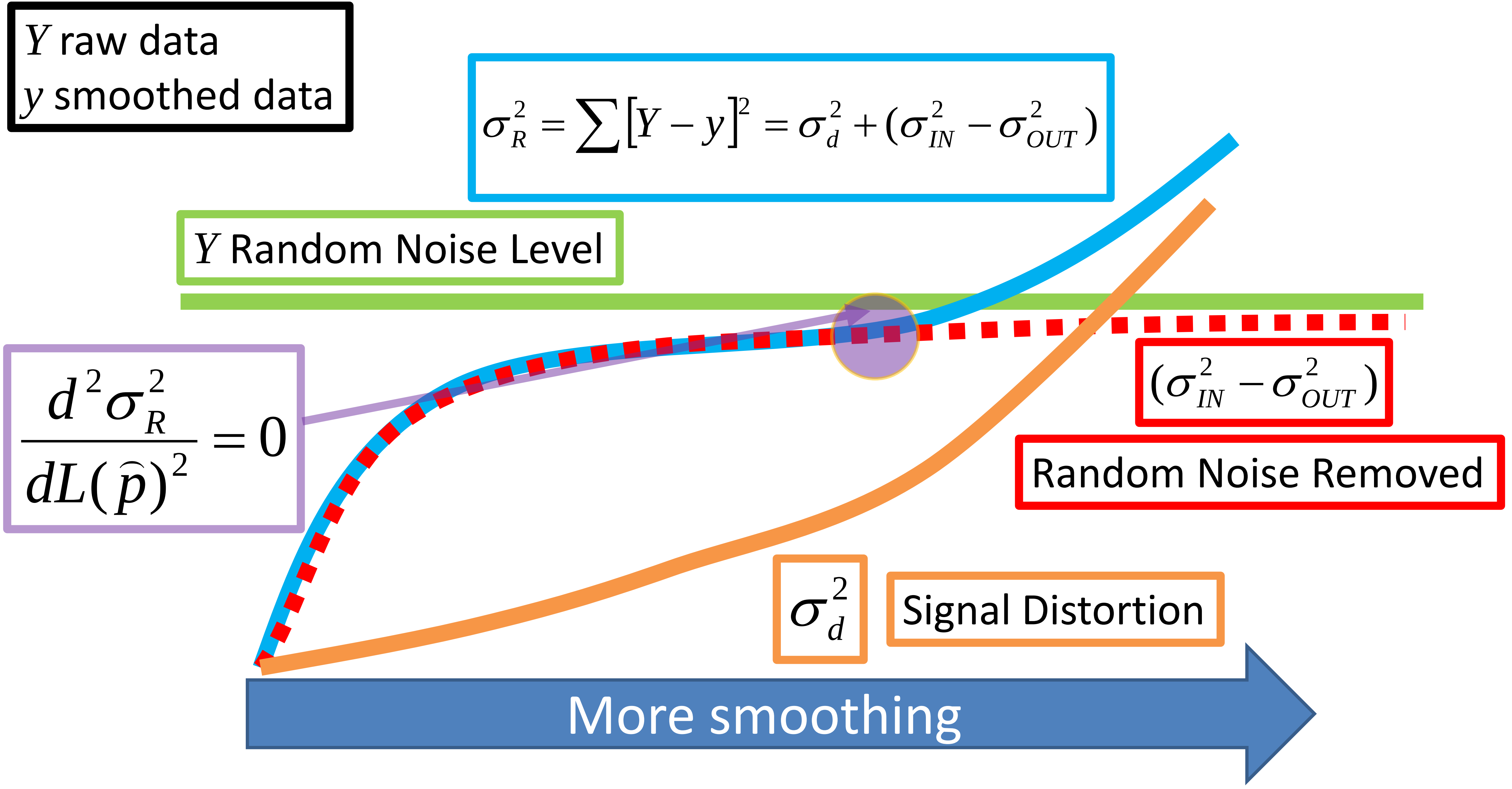
Y raw data
y smoothed data
$\sigma_R^2 = \sum [Y - y]^2 = \sigma_d^2 + (\sigma_{IN}^2 - \sigma_{OUT}^2)$
Y Random Noise Level
$\frac{d^2 \sigma_R^2}{dL(\widehat{p})^2} = 0$
$(\sigma_{IN}^2 - \sigma_{OUT}^2)$
Random Noise Removed
σ_d^2
Signal Distortion
More smoothing

Elastic/Raman Signal simulations with actual parameters but without ND filters: too much photons for low range…

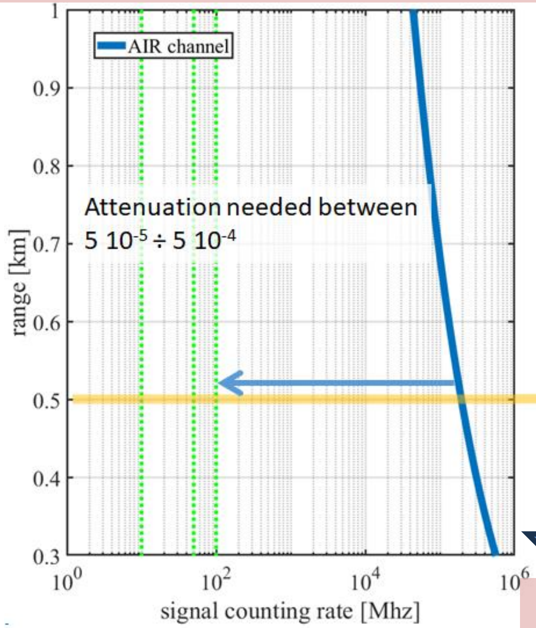

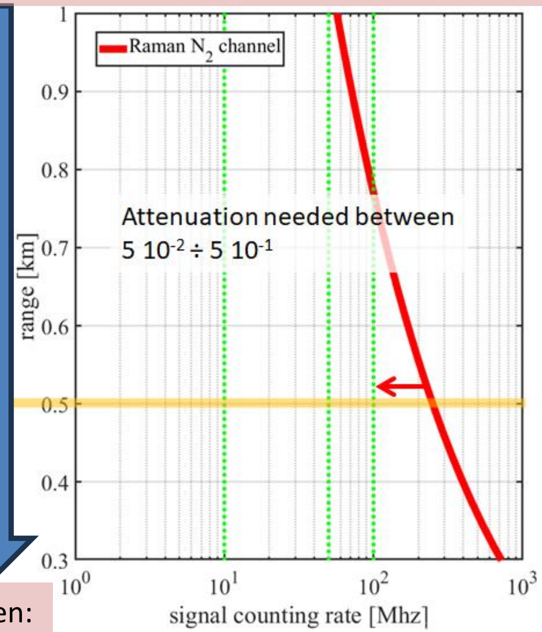

Then:

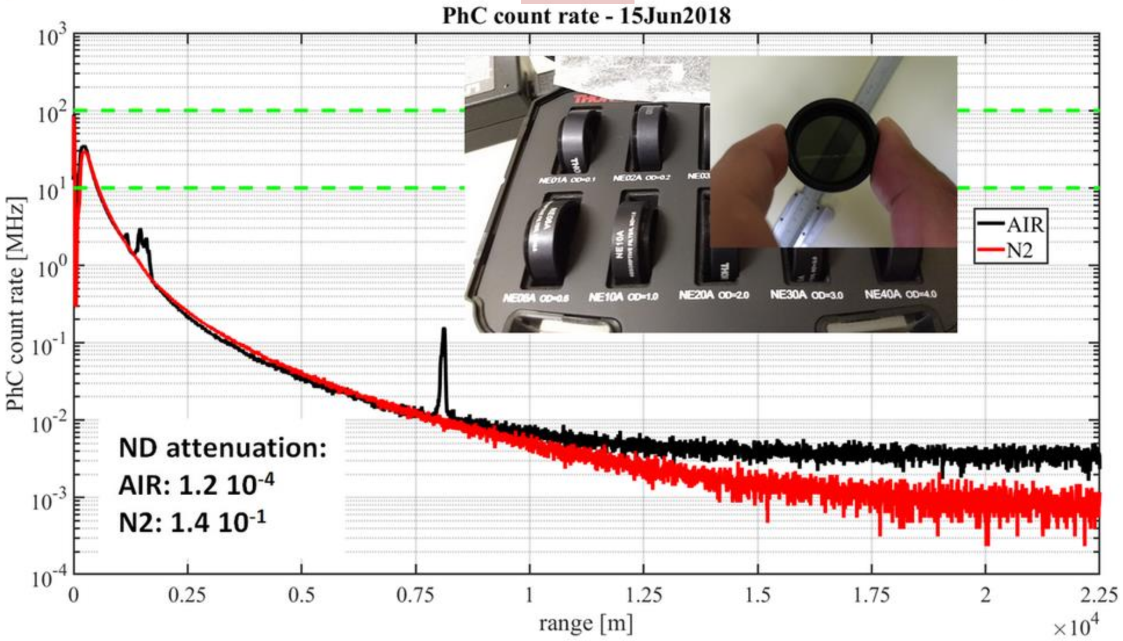

Lidar Signal simulator

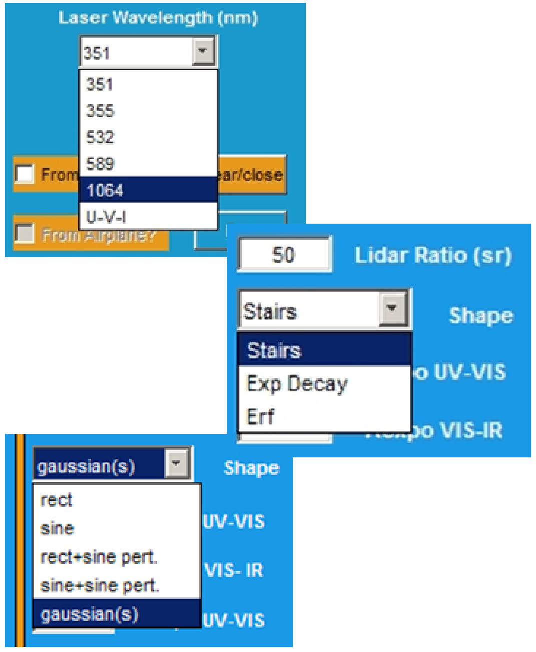

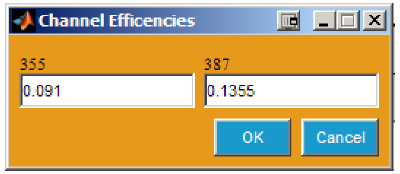

Molecular density profile

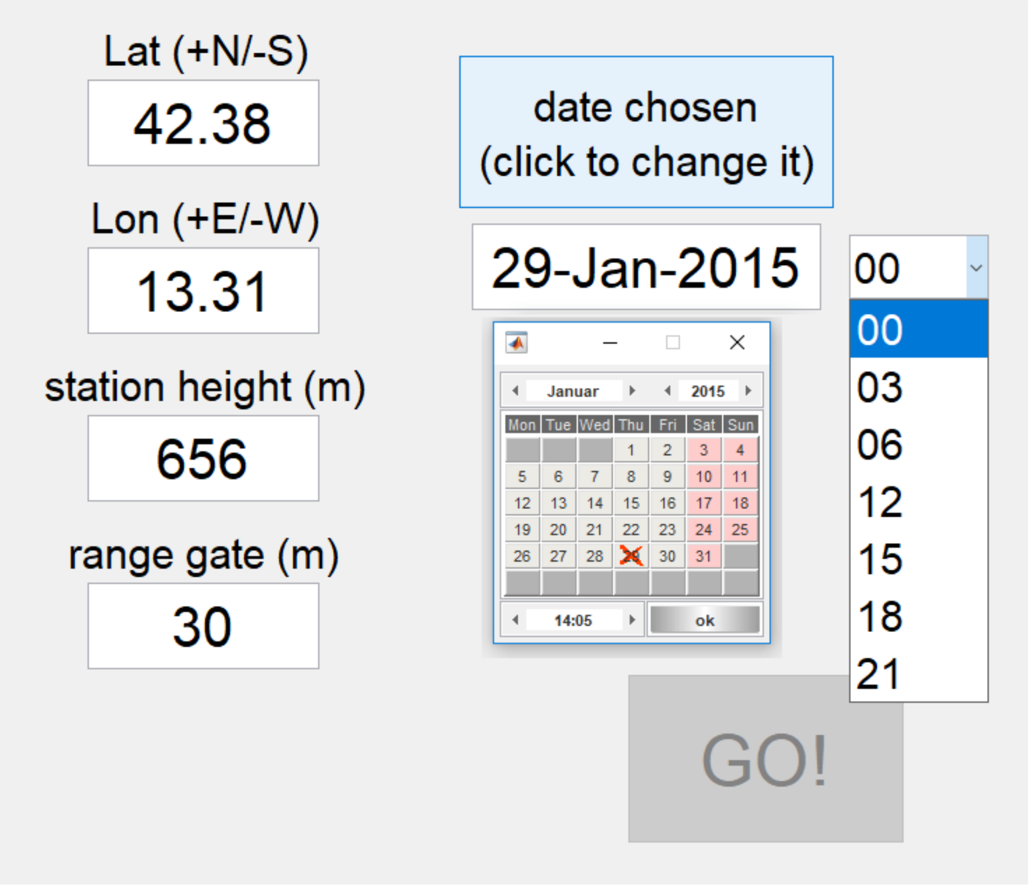

GDAS DATA ON A GRID 1°x1°

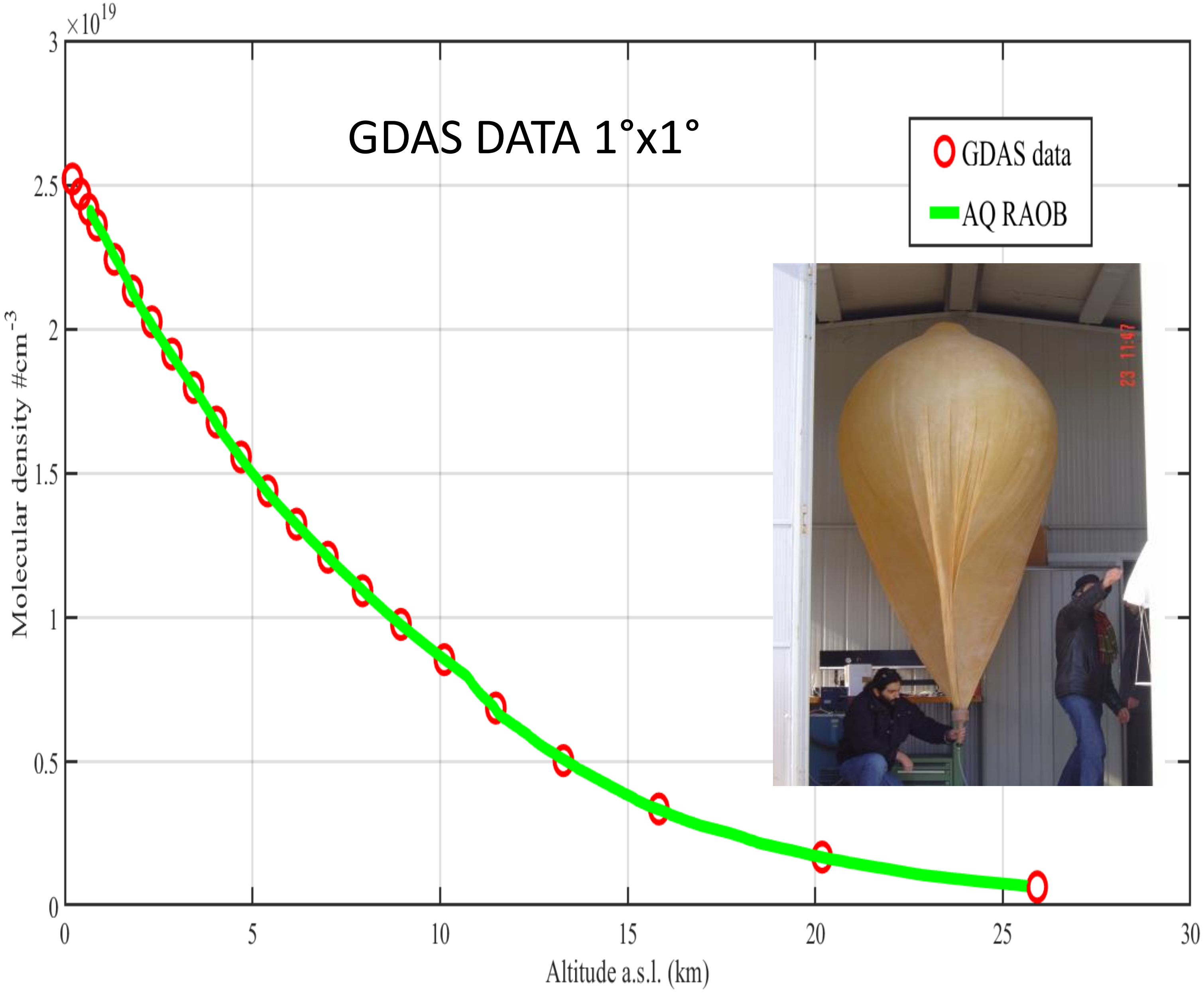

Rayleigh Fit Test

A lidar signal normalized by the attenuated molecular backscatter coefficient. Regions of pure molecular scattering can be identified by the good agreement between the Rayleigh fit and the observed attenuated molecular backscatter coefficient.

No significative differences in the far range: OK

Freudenthaler, V.: Lidar Rayleigh-fit criteria, in: EARLINET-ASOS 7th Workshop, available at: http://nbnresolving.de/urn/resolver.pl?urn=nbn:de:bvb:19-epub-12970-6, 2009.

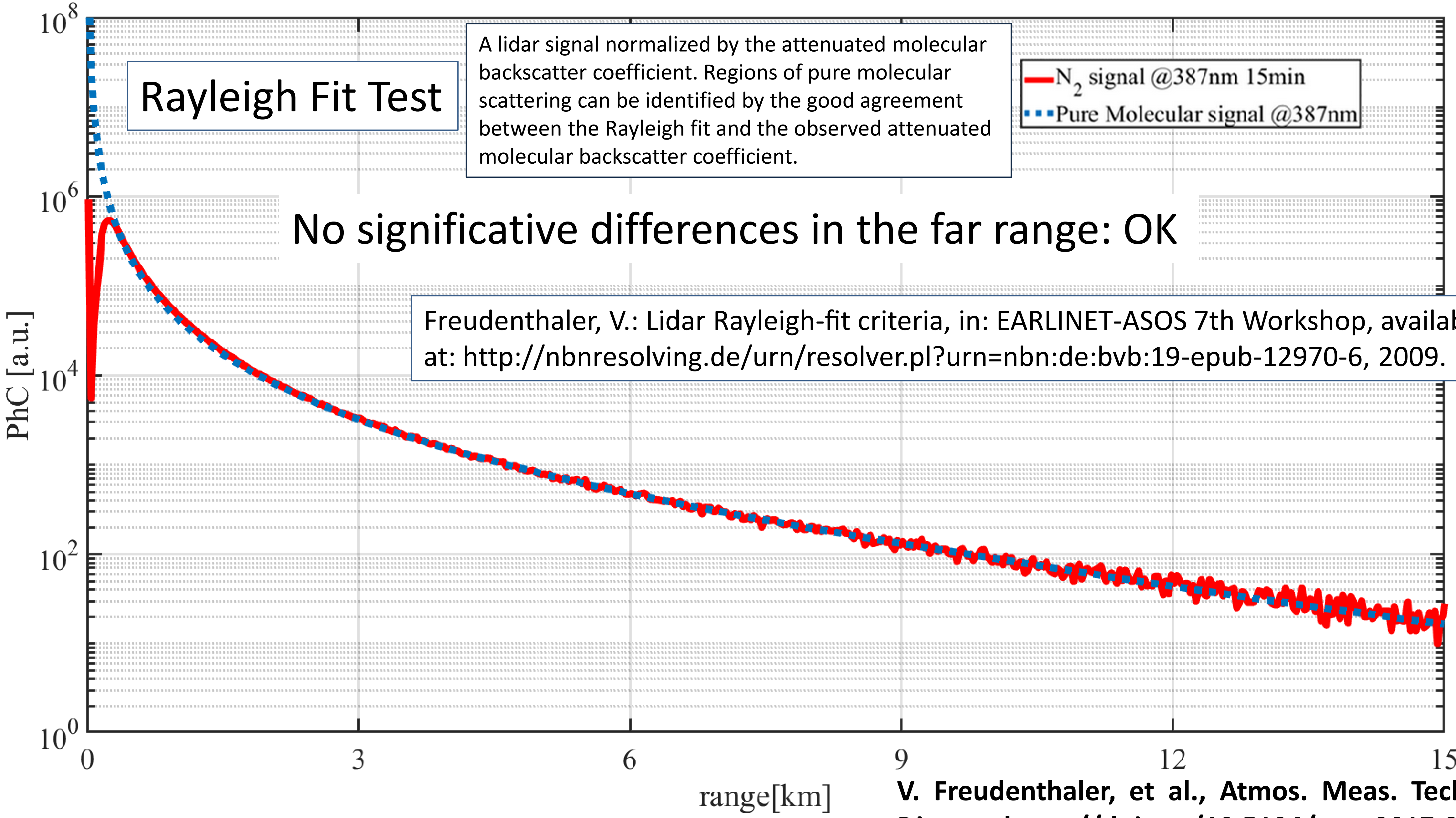

V. Freudenthaler, et al., Atmos. Meas. Tech. Discuss.,https://doi.org/10.5194/amt-2017-395

ZEMAX© simulation for G(s)

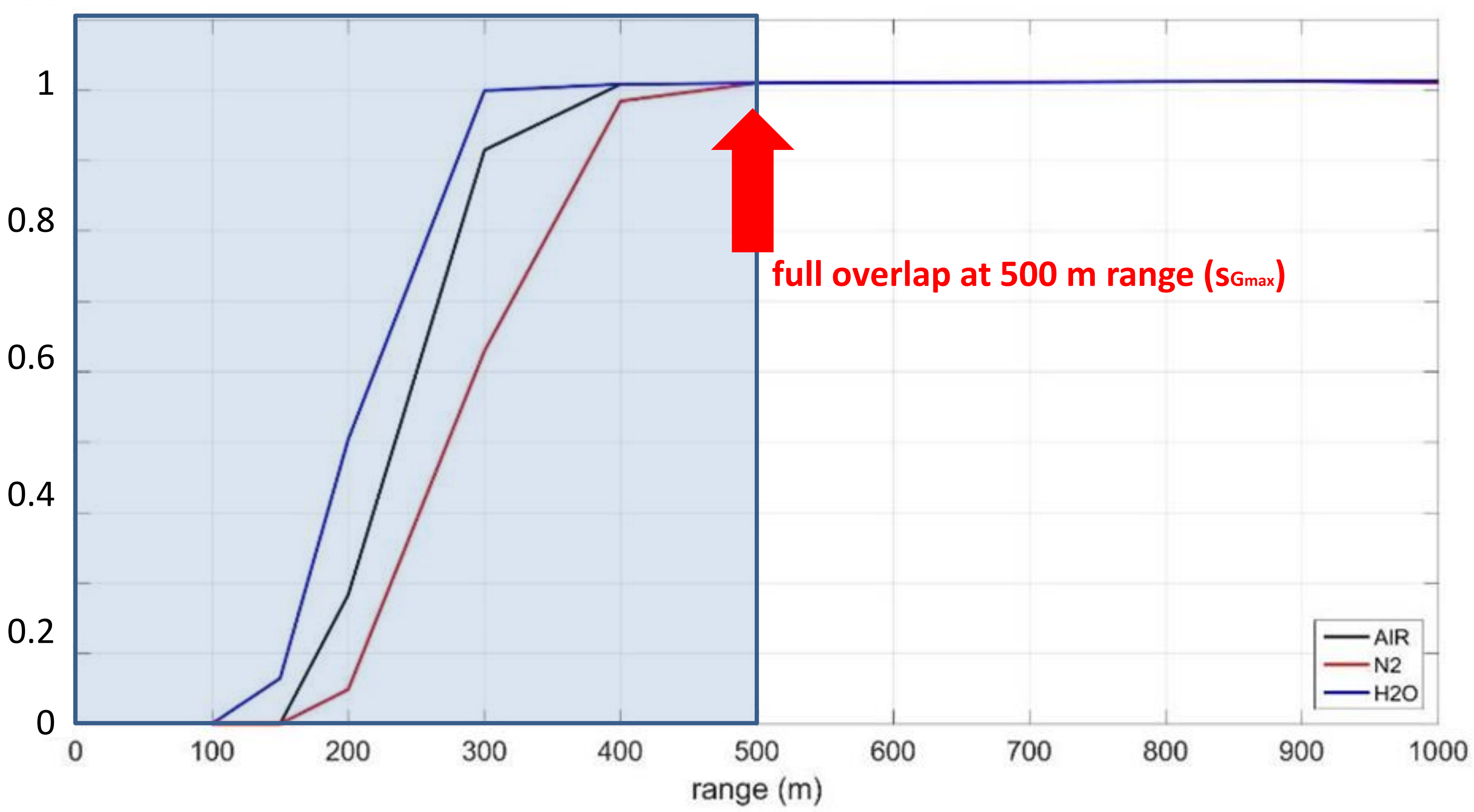

r G(s)

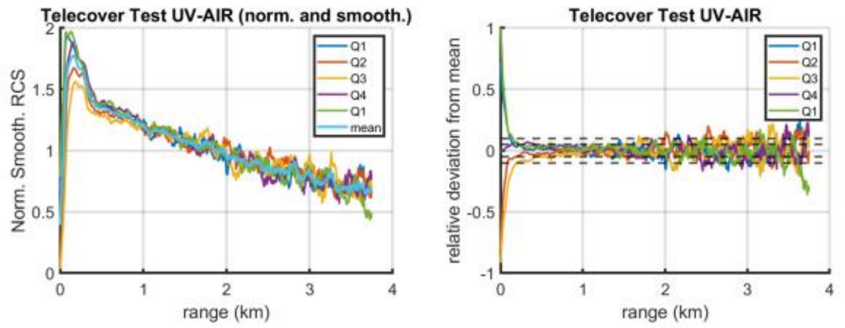

Figure 6.30: Quadrant telecover test of channel UV-AIR.

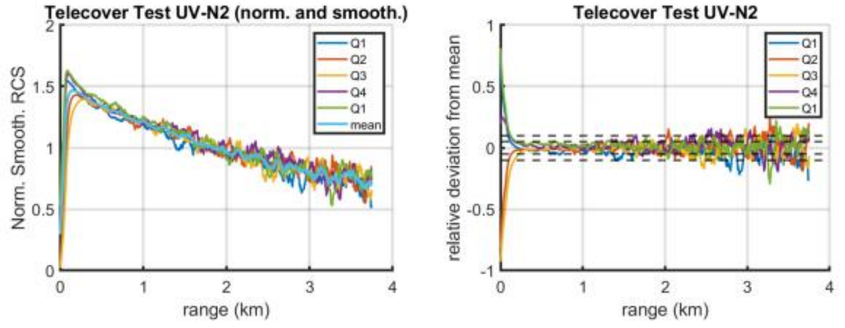

Figure 6.31: Quadrant telecover test of channel UV-N2.

Deviations of the near range signals from different parts of the telescope and the comparison of such deviations of different lidar channels and with theoretical ray-tracing simulations can reveal the distance of full overlap and possible reasons for the deviations from the ideal case.

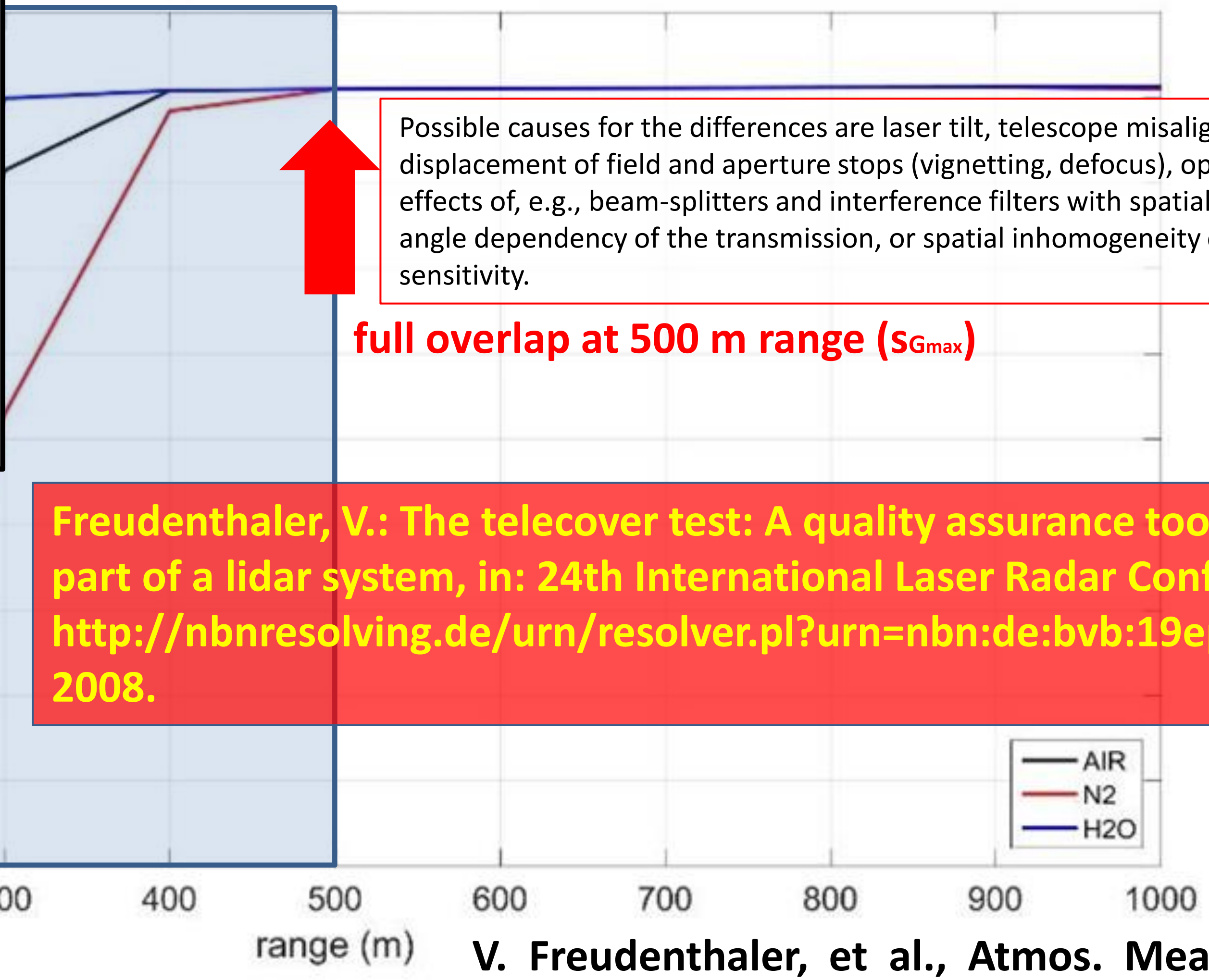

Possible causes for the differences are laser tilt, telescope misalignments, displacement of field and aperture stops (vignetting, defocus), optical coating effects of, e.g., beam-splitters and interference filters with spatial inhomogeneity or angle dependency of the transmission, or spatial inhomogeneity of the detector sensitivity.

full overlap at 500 m range (s_{Gmax})

Freudenthaler, V.: The telecover test: A quality assurance tool for the optical part of a lidar system, in: 24th International Laser Radar Conference, http://nbnresolving.de/urn/resolver.pl?urn=nbn:de:bvb:19epub-12958-1, 2008.

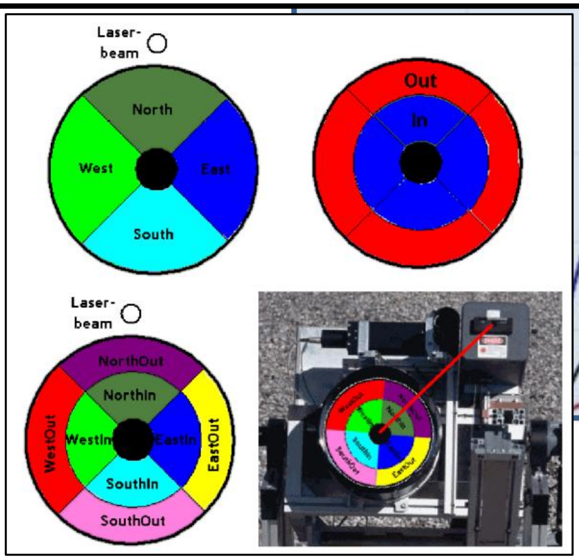

V. Freudenthaler, et al., Atmos. Meas. Tech. Discuss.,https://doi.org/10.5194/amt-2017-395

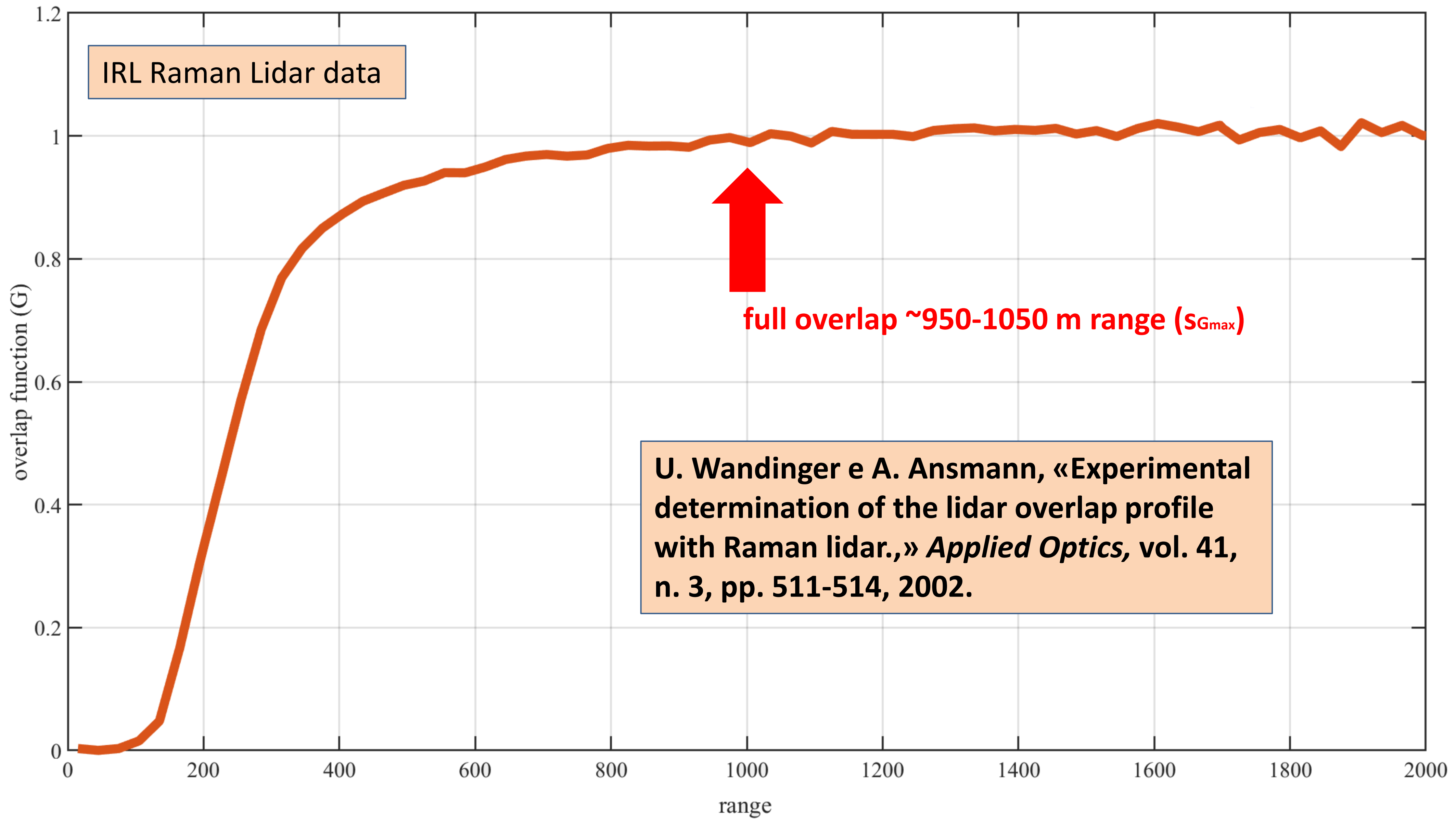
IRL Raman Lidar data
full overlap ~950-1050 m range (s_{Gmax})
U. Wandinger e A. Ansmann, «Experimental determination of the lidar overlap profile with Raman lidar.,» *Applied Optics*, vol. 41, n. 3, pp. 511-514, 2002.
overlap function (G)
range
0
0.2
0.4
0.6
0.8
1
1.2
200
400
600
800
1000
1200
1400
1600
1800
2000

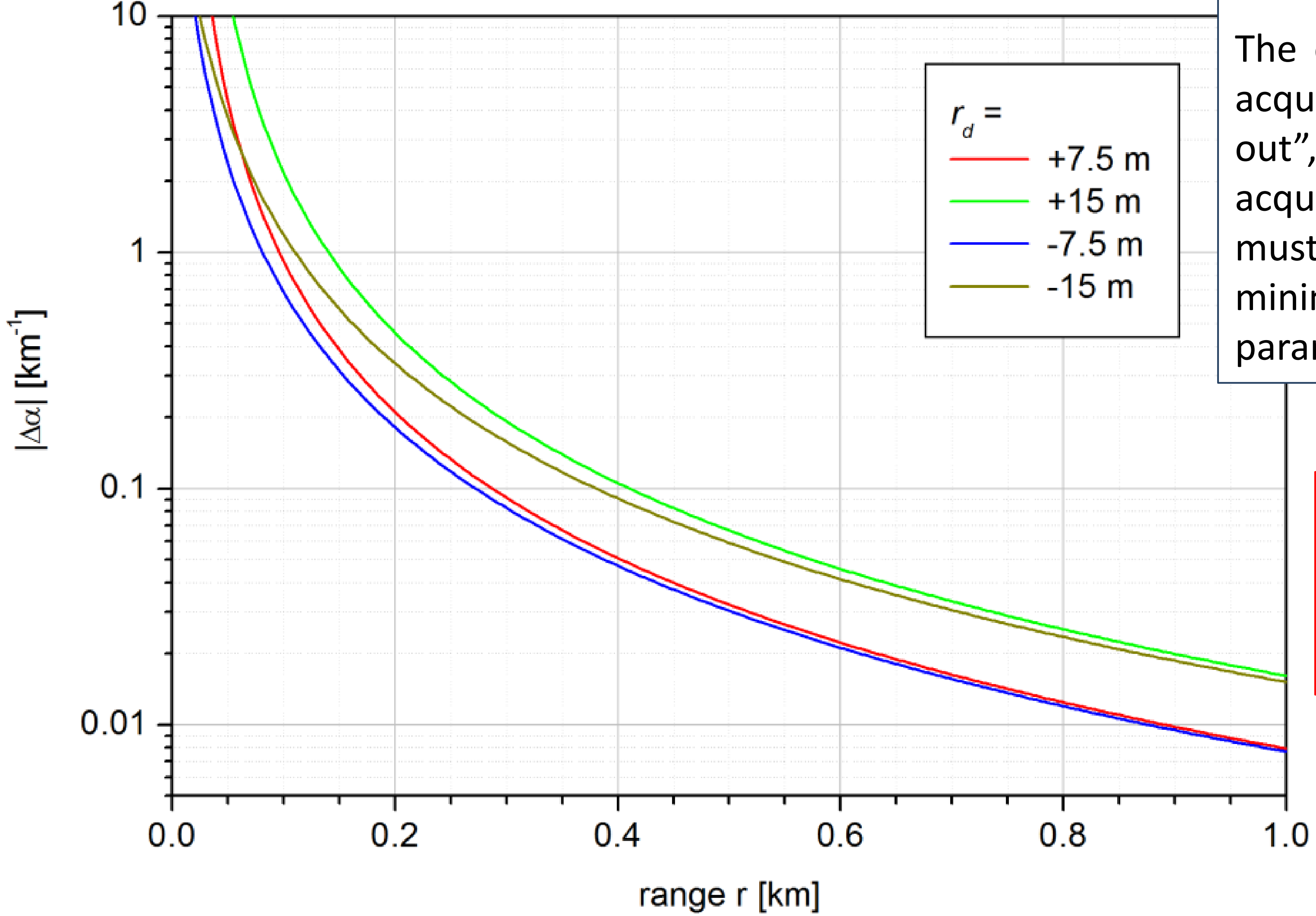

Zero-bin delay

The delay between the trigger, that also starts the acquisition board measurements, and the "laser out", that establish the position of the first acquisition. This is an important parameter that must be determined with sufficient precision to minimize systematic uncertainty in the optical parameter's retrieval.

$$\frac{d}{dr_d}\alpha_p(r,r_d) \approx -\frac{2}{1+f_p}\frac{1}{(r-r_d)^2}$$

A non-accurate measurements can cause large errors in the AE and AOD.
V. Freudenthaler, et al., Atmos. Meas. Tech. Discuss.,https://doi.org/10.5194/amt-2017-395.

The trace of the trigger and of the photo diode shows the overall delay (Δt=120ns±2.5ns), but for "trigger – laser out delay" ($\Delta\tau_L$), we must take into account the delays introduced by the cables and the delay introduced by the transit time characteristic of the photo diode and also of the distance between the photo diode and the laser head:

$\Delta\tau_L = \Delta t$ [measured with the oscilloscope] +

– [photodiode transit time (3 ns ± 2 ns)] +

[+ 1.5 m BNC cable (7.5 ± 1 ns) - 1.5 m BNC cable (7.5 ± 1 ns)]

+

- [laser path in air (2 ns)]

The resulting is $\Delta\tau_L$=115 ns ± 5ns.

To reduce the «zero bin» indetermination even the smallest sources of delays must be taken into account.

MEASUREMENTS WITH FAST PHOTODIODE of the laser emission at laser exit

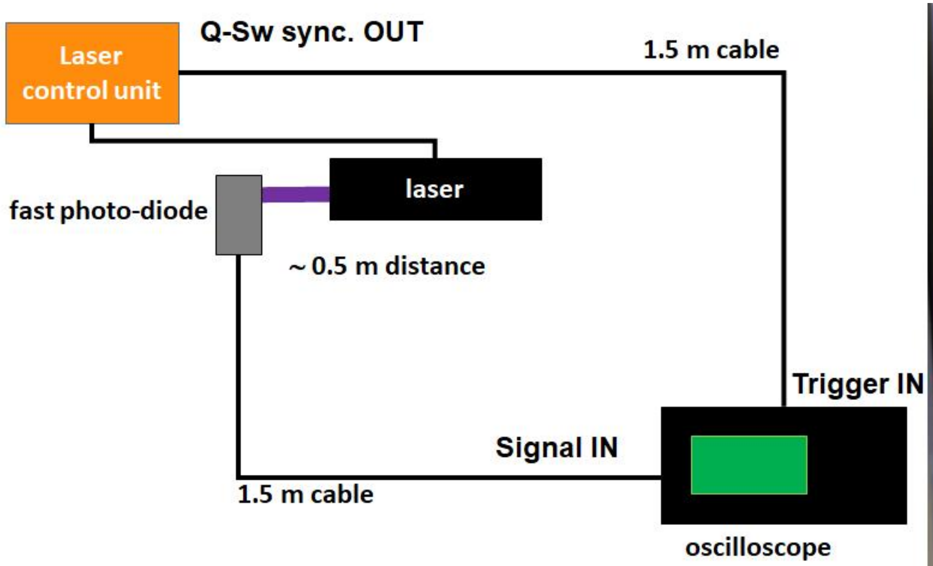

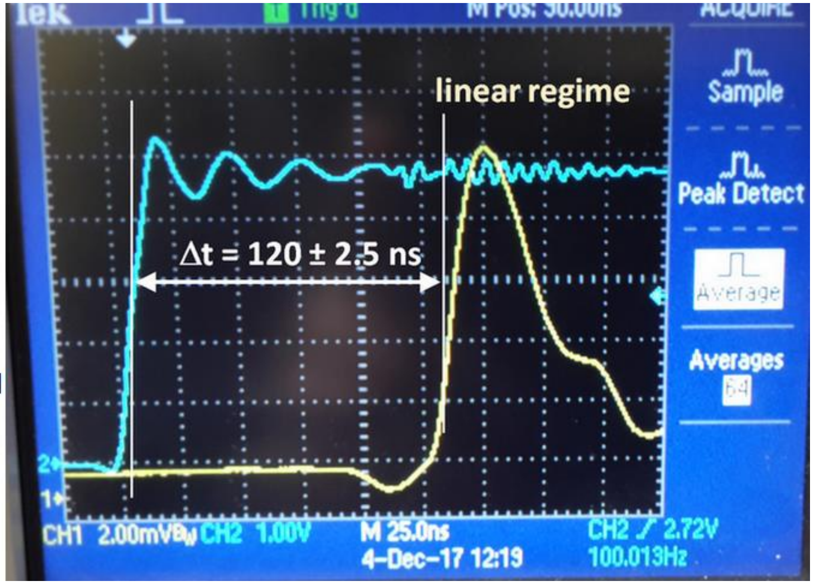

SUMMARY PhC

Q switch sync out and laser pulse emission at DAQ

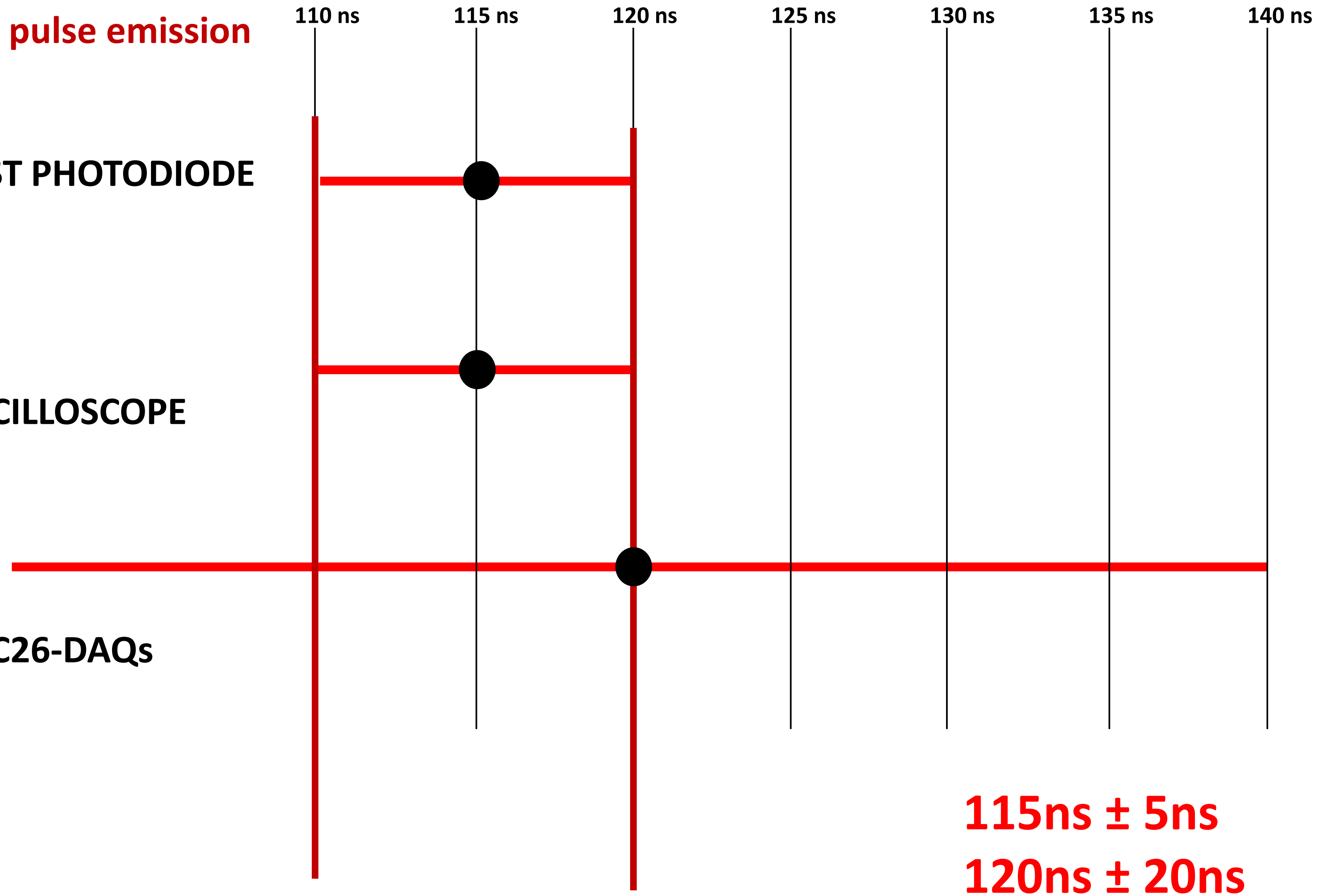

MEASUREMENTS WITH FAST PHOTODIODE
of laser emission

MEASUREMENTS WITH OSCILLOSCOPE
of local reflections/echoes

MEASUREMENTS WITH APC26-DAQs
of local reflections/echoes

115ns ± 5ns
120ns ± 20ns

110÷120 ns

Statistical uncertainties

Error propagation or ...

$$\Delta\beta_p^{ran}(r,\lambda_0) = \sqrt{\left(\frac{\partial\beta_p(r,\lambda_0)}{\partial P(r,\lambda_0)}\cdot\Delta P(r,\lambda_0)\right)^2+\left(\frac{\partial\beta_p(r,\lambda_0)}{\partial P(r_0,\lambda_0)}\cdot\Delta P(r_0,\lambda_0)\right)^2 +\left(\frac{\partial\beta_p(r,\lambda_0)}{\partial P(r,\lambda_R)}\cdot\Delta P(r,\lambda_R)\right)^2+\left(\frac{\partial\beta_p(r,\lambda_0)}{\partial P(r_0,\lambda_R)}\cdot\Delta P(r_0,\lambda_R)\right)^2}$$

P=lidar signal (E&R)

The Monte Carlo (MC) method is based on the random generation of new lidar signals. Each range bin of these signals is considered as a sample element of a probability distribution with mean value and standard deviation that corresponds to the value and uncertainty of signal profiles.
The extracted lidar signals are then processed with the same algorithm to produce a set of solutions. The standard deviation of these solutions is finally used as profile of the statistical error.
Mattis at al., Atmos. Meas. Tech., 9, 3009–3029, 2016

S. Groß et al., Lidar ratio of Saharan dust over Cape Verde Islands: Assessment and error calculation, JGR: Atmospheres, vol. 116, n. D15, 2011.

Statistical uncertainties

Error propagation or ...

$$\Delta\beta_p^{ran}(r,\lambda_0) = \sqrt{\left(\frac{\partial\beta_p(r,\lambda_0)}{\partial P(r,\lambda_0)}\cdot\Delta P(r,\lambda_0)\right)^2+\left(\frac{\partial\beta_p(r,\lambda_0)}{\partial P(r_0,\lambda_0)}\cdot\Delta P(r_0,\lambda_0)\right)^2 +\left(\frac{\partial\beta_p(r,\lambda_0)}{\partial P(r,\lambda_R)}\cdot\Delta P(r,\lambda_R)\right)^2+\left(\frac{\partial\beta_p(r,\lambda_0)}{\partial P(r_0,\lambda_R)}\cdot\Delta P(r_0,\lambda_R)\right)^2}$$

P=lidar signal (E&R)

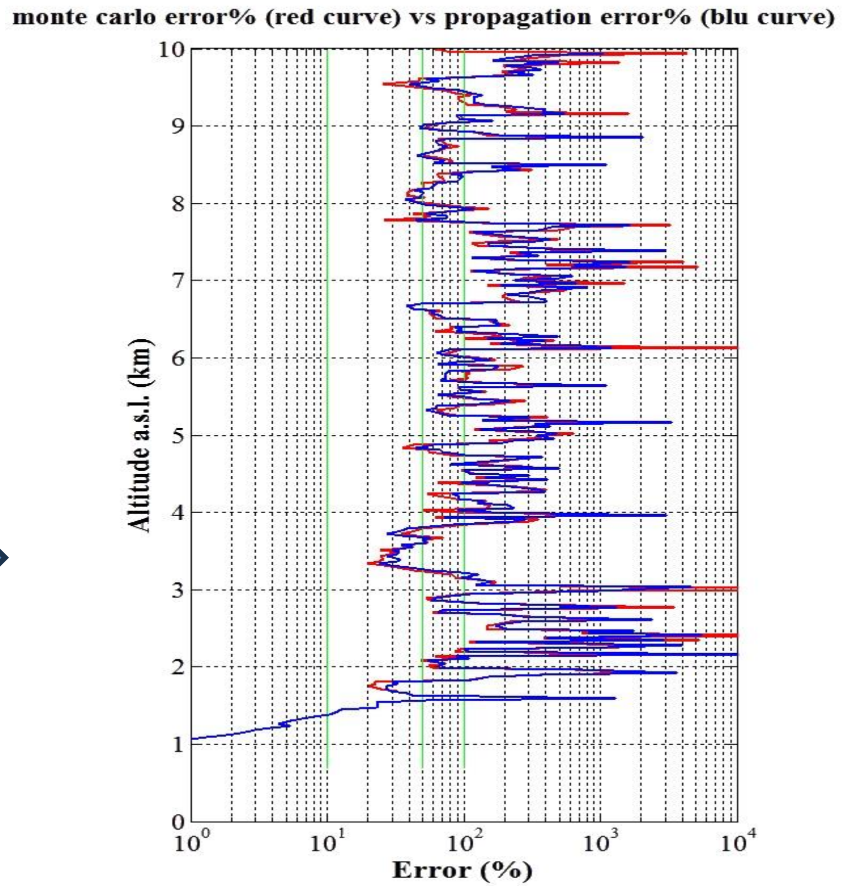

Monte Carlo method and error propagation provide comparable error profiles in case of Raman extinction and Raman backscatter retrievals.

Mattis at al., Atmos. Meas. Tech., 9, 3009–3029, 2016

S. Groß et al., Lidar ratio of Saharan dust over Cape Verde Islands: Assessment and error calculation, JGR: Atmospheres, vol. 116, n. D15, 2011.

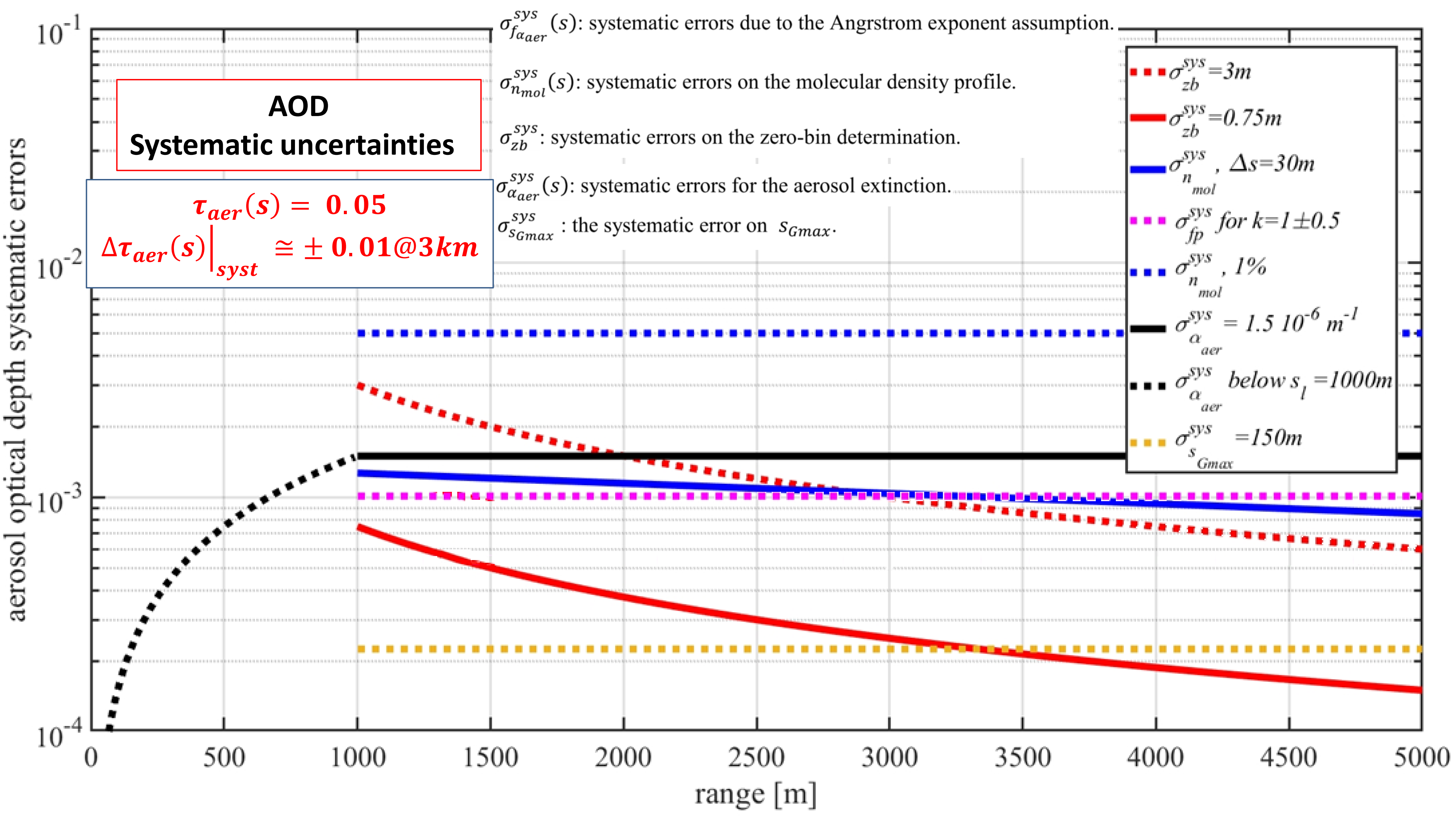
AOD
Systematic uncertainties
$\tau_{aer}(s) = 0.05$
$\Delta\tau_{aer}(s)\big|_{syst} \cong \pm 0.01@3km$
$\sigma^{sys}_{f_{\alpha aer}}(s)$: systematic errors due to the Angrstrom exponent assumption.
$\sigma^{sys}_{n_{mol}}(s)$: systematic errors on the molecular density profile.
σ^{sys}_{zb}: systematic errors on the zero-bin determination.
$\sigma^{sys}_{\alpha_{aer}}(s)$: systematic errors for the aerosol extinction.
$\sigma^{sys}_{s_{Gmax}}$: the systematic error on s_{Gmax}.
σ^{sys}_{zb}=3m
σ^{sys}_{zb}=0.75m
$\sigma^{sys}_{n_{mol}}$, Δs=30m
σ^{sys}_{fp} for k=1±0.5
$\sigma^{sys}_{n_{mol}}$, 1%
$\sigma^{sys}_{\alpha_{aer}}$ = 1.5 10^{-6} m^{-1}
$\sigma^{sys}_{\alpha_{aer}}$ below s_1 =1000m
$\sigma^{sys}_{s_{Gmax}}$ =150m
aerosol optical depth systematic errors
10^{-1}
10^{-2}
10^{-3}
10^{-4}
0
500
1000
1500
2000
2500
3000
3500
4000
4500
5000
range [m]

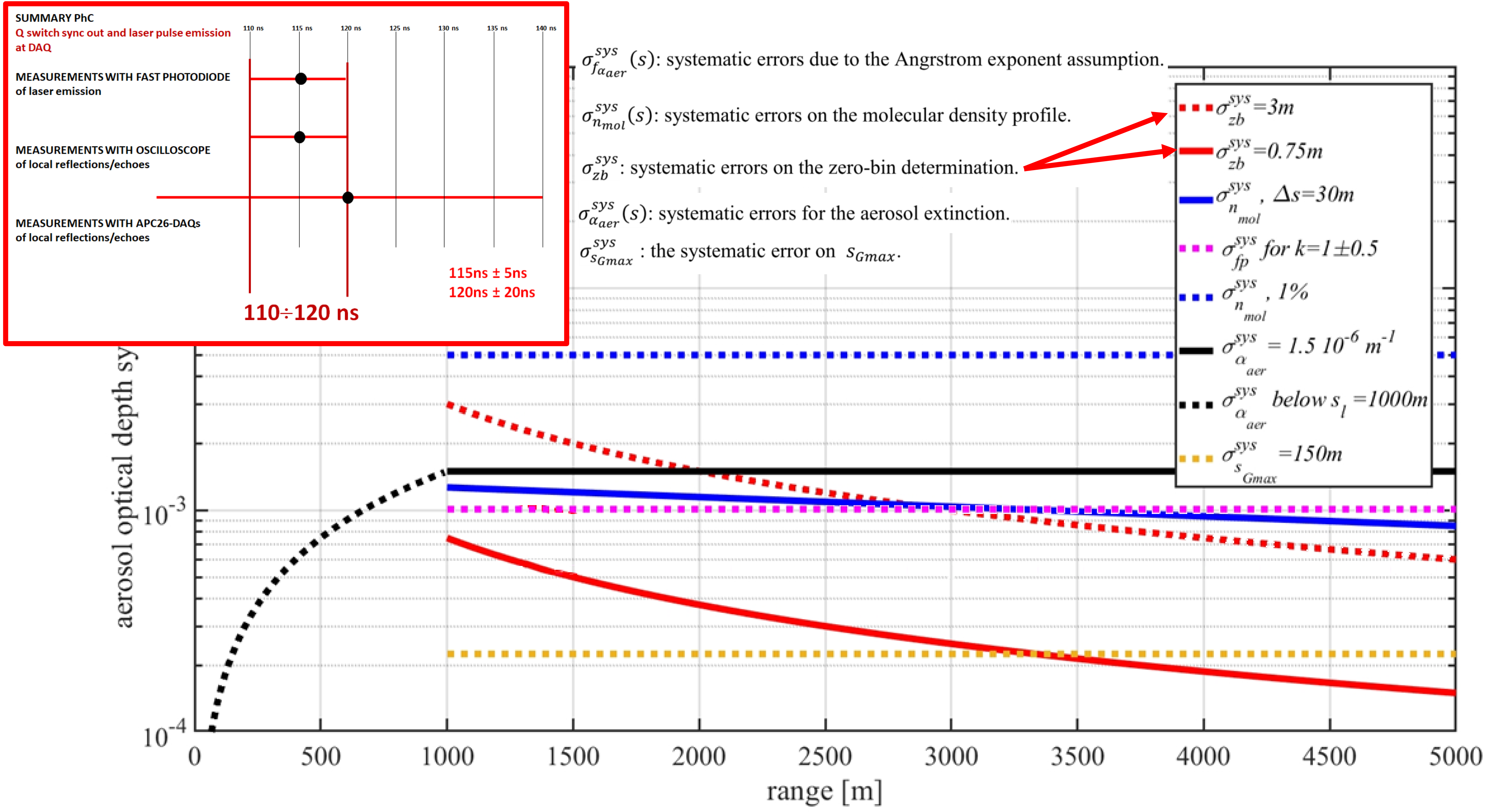
SUMMARY PhC
Q switch sync out and laser pulse emission at DAQ
110 ns
115 ns
120 ns
125 ns
130 ns
135 ns
140 ns
MEASUREMENTS WITH FAST PHOTODIODE of laser emission
MEASUREMENTS WITH OSCILLOSCOPE of local reflections/echoes
MEASUREMENTS WITH APC26-DAQs of local reflections/echoes
115ns ± 5ns
120ns ± 20ns
110÷120 ns
$\sigma^{sys}_{f_{\alpha aer}}(s)$: systematic errors due to the Angrstrom exponent assumption.
$\sigma^{sys}_{n_{mol}}(s)$: systematic errors on the molecular density profile.
σ^{sys}_{zb}: systematic errors on the zero-bin determination.
$\sigma^{sys}_{\alpha_{aer}}(s)$: systematic errors for the aerosol extinction.
$\sigma^{sys}_{s_{Gmax}}$: the systematic error on s_{Gmax}.
σ^{sys}_{zb}=3m
σ^{sys}_{zb}=0.75m
$\sigma^{sys}_{n_{mol}}$, Δs=30m
σ^{sys}_{fp} for k=1±0.5
$\sigma^{sys}_{n_{mol}}$, 1%
$\sigma^{sys}_{\alpha_{aer}}$ = 1.5 10^{-6} m^{-1}
$\sigma^{sys}_{\alpha_{aer}}$ below s_l=1000m
$\sigma^{sys}_{s_{Gmax}}$=150m
aerosol optical depth sy
10^{-3}
10^{-4}
0
500
1000
1500
2000
2500
3000
3500
4000
4500
5000
range [m]

For $k = 1 \pm 0.5$, the relative systematic error on the extinction/AOD is only about 2%, which can be further reduced if a more precise knowledge of the aerosol type is available.

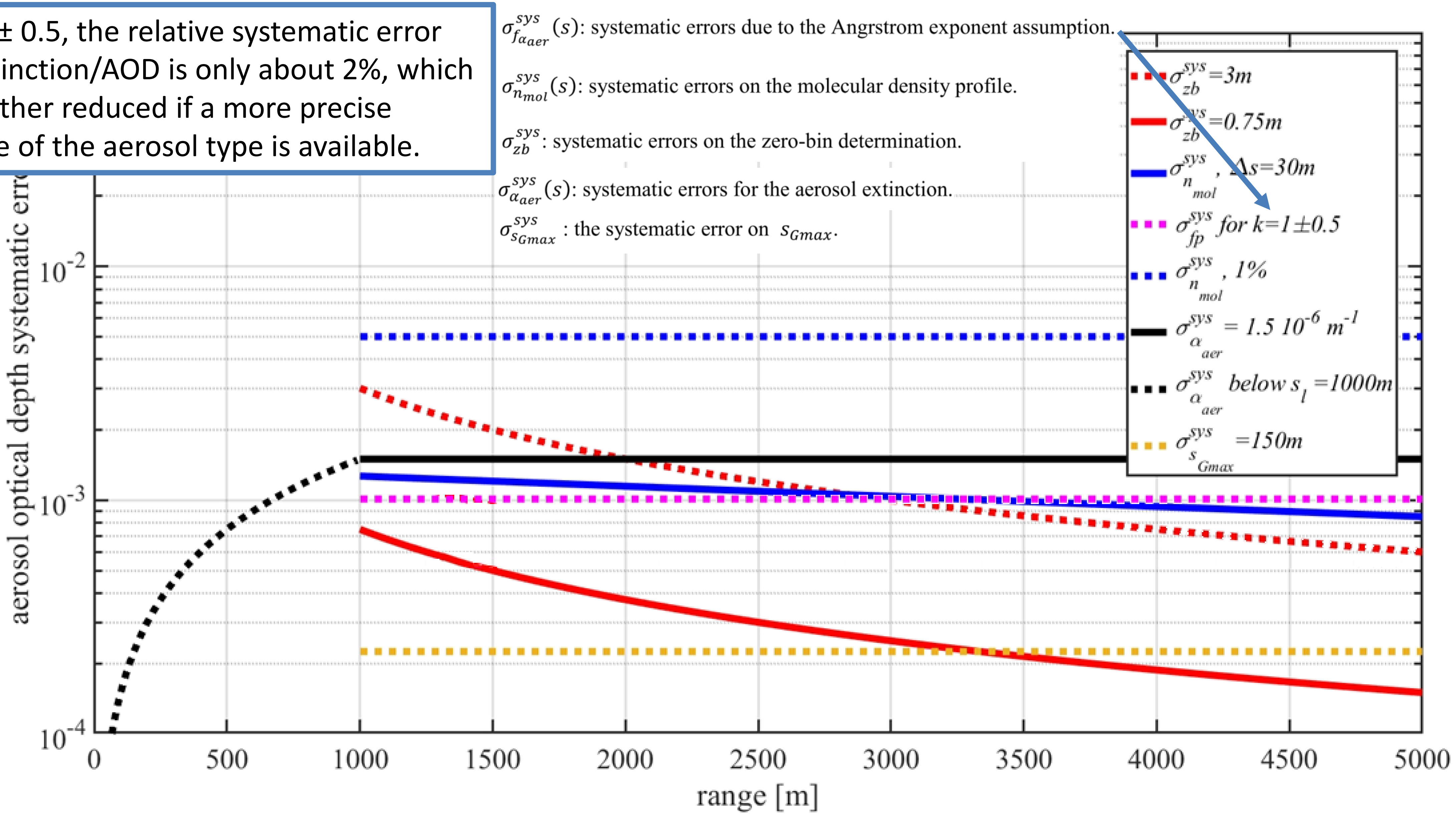

M. Will, Astropart. Phys., vol. 35, pp. 591-607, 2012. 1%
S. Groß et al., JGR: Atmos., vol. 116, n. D15, 2011. 2%

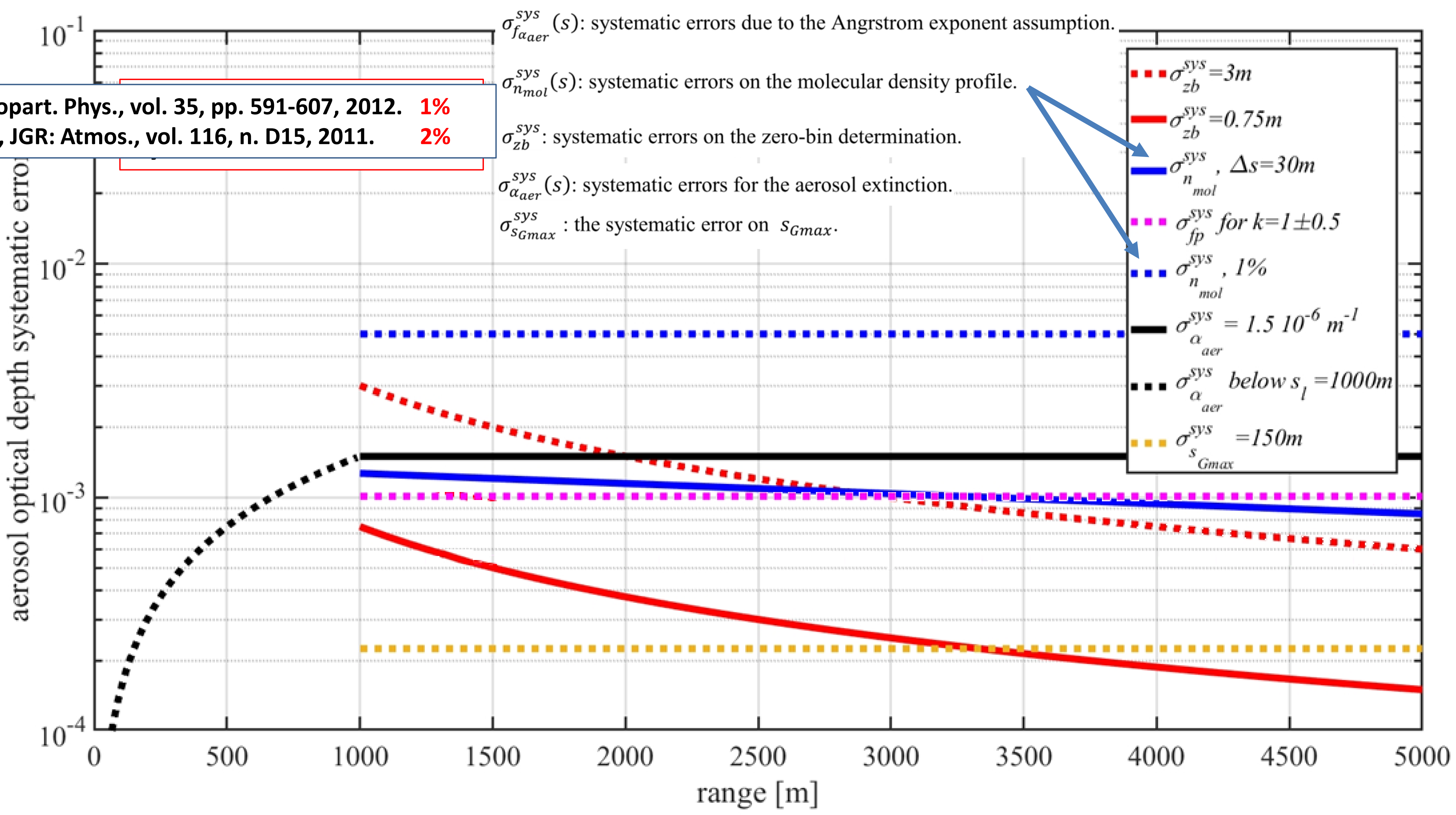

The systematic uncertainties caused for the assumed aerosol extinction for in the not full overlap region, estimated from the uncertainties analysis of the extinction.

The systematic uncertainties on the retrieval of the full overlap range (S_{Gmax}) (retrieval methods, temperature etc…)

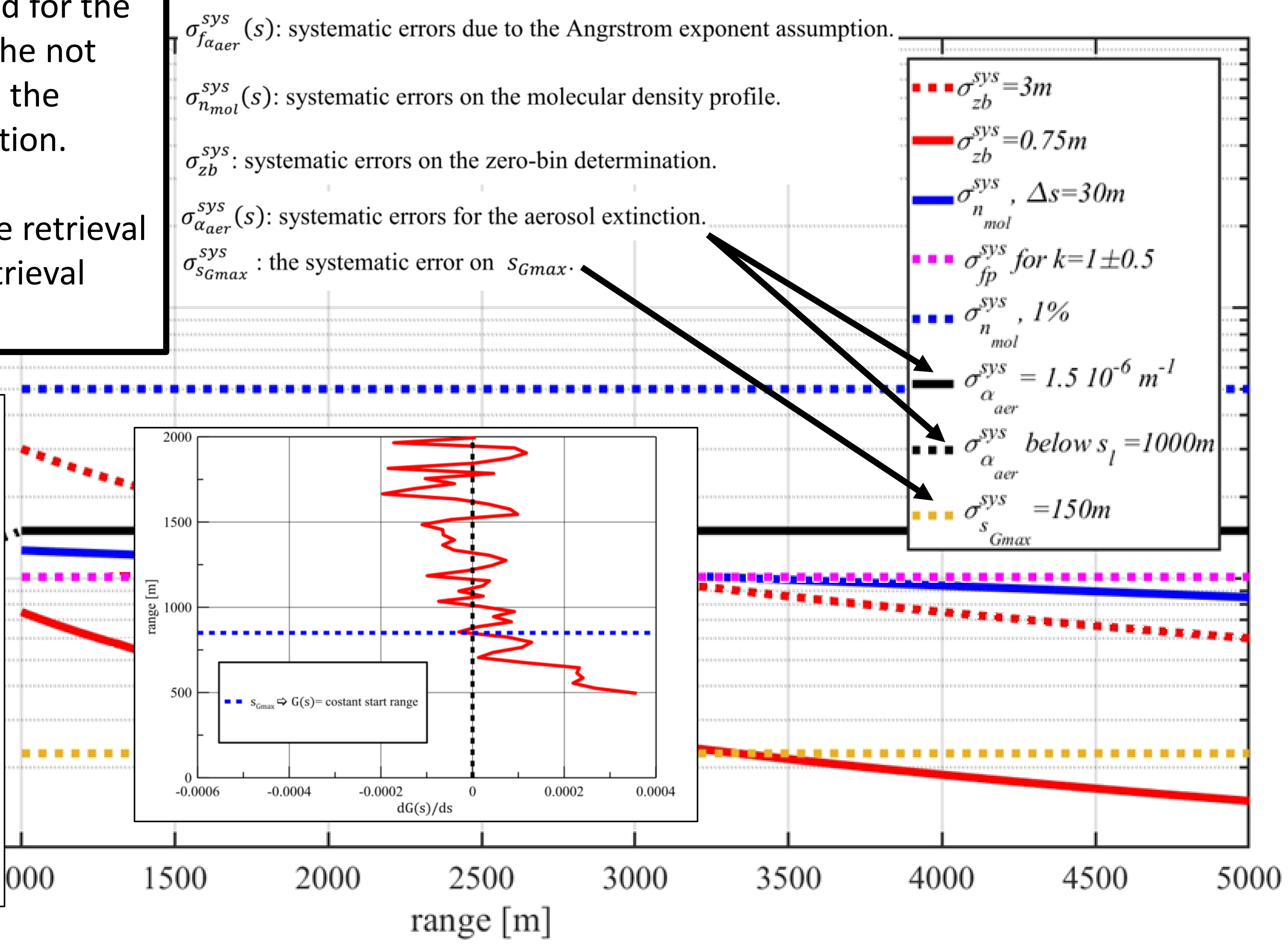

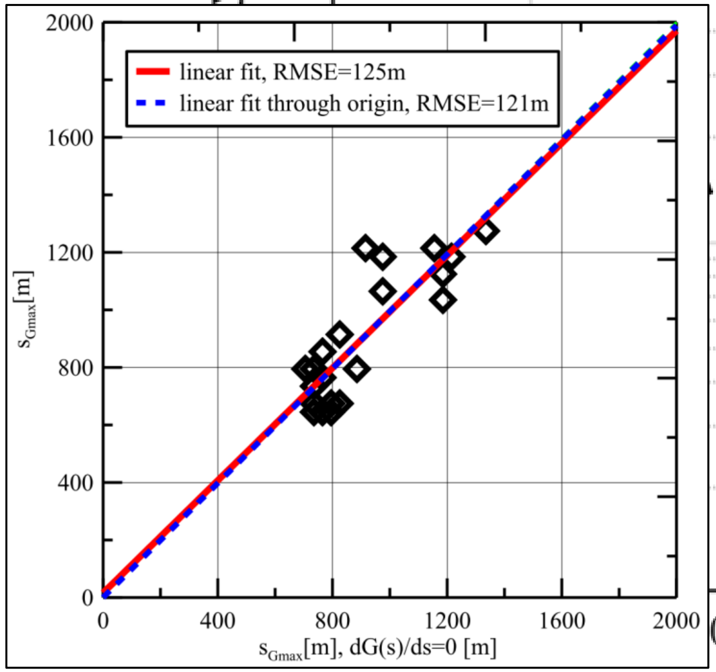

Raman LIDAR @ UNIVAQ.

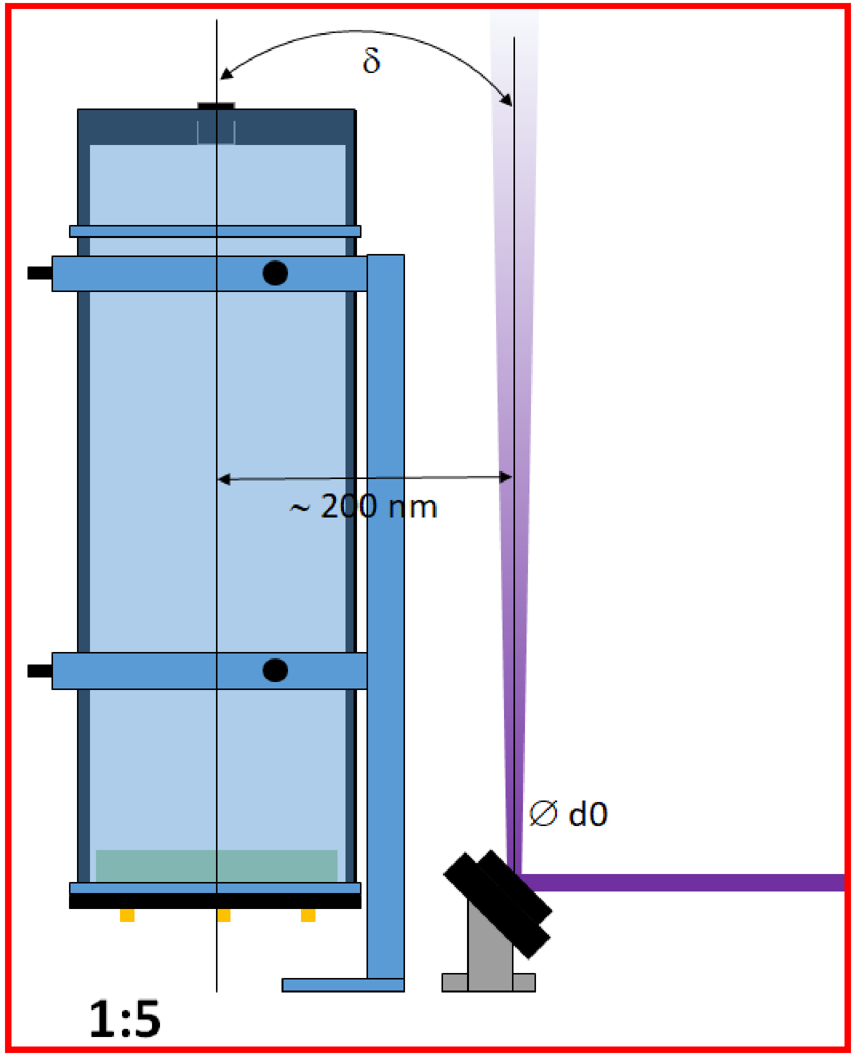

TOP VIEW

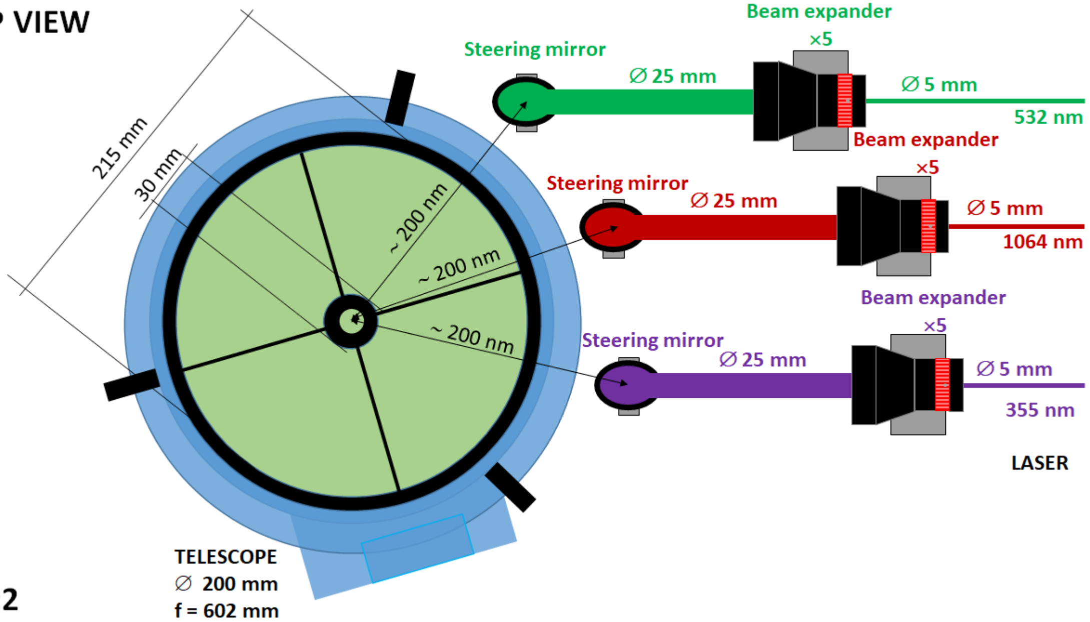

Aerosol and water Raman UV LIDAR at CETEMPS, L'Aquila, now UV, VIS, IR LIDAR

FIBER BUNDLE

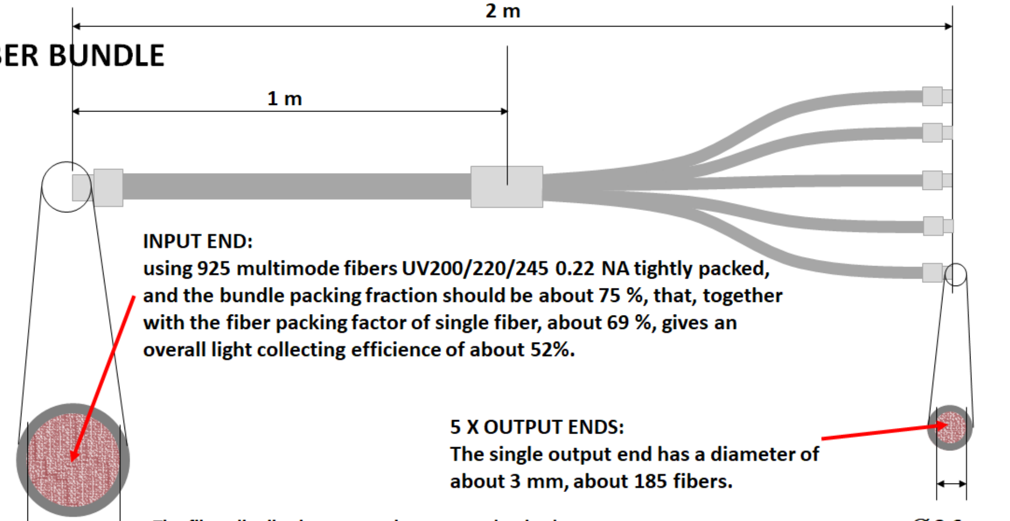

no scale

The fiber distribution among legs are randomized.
The end surfaces should have been polished at the best (0.3 µm).
The bundle and the legs should are in a stainless steel tubing and terminated with sleeves.
An epoxy adhesive is used, it has optical and physical properties similar to EPO-TEK® 353°.

Aerosol and water Raman UV LIDAR at CETEMPS, L'Aquila, now UV, VIS, IR LIDAR

Raman LIDAR @ UNIVAQ.

Center of Excellence
CETEMPS
Telesensing of Environment and Model Prediction of Severe events

DSFC
Dipartimento di Scienze Fisiche e Chimiche

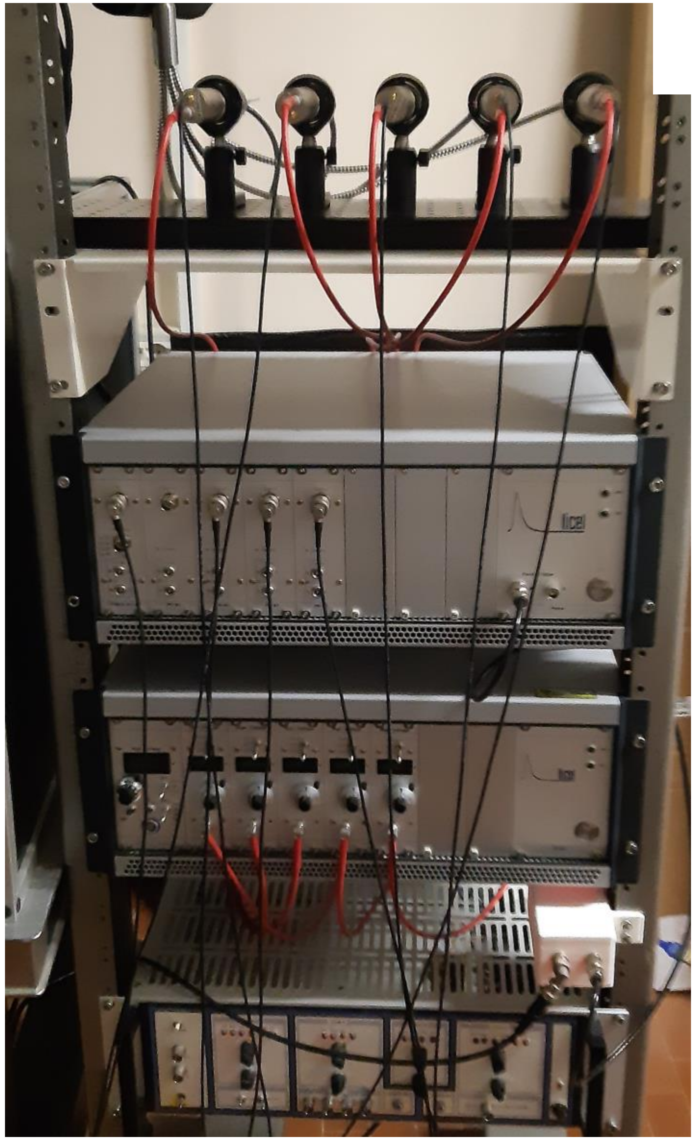

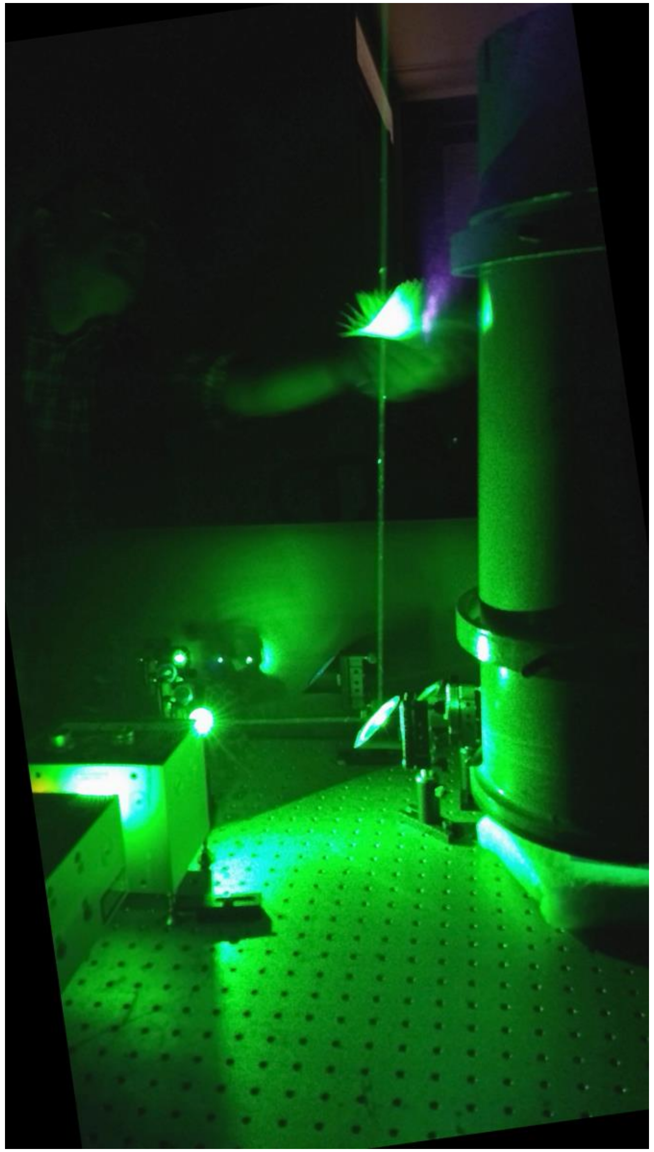

Raman LIDAR @ UNIVAQ.

Center of Excellence
CETEMPS
Telesensing of Environment and Model Prediction of Severe events

DSFC Dipartimento di Scienze Fisiche e Chimiche

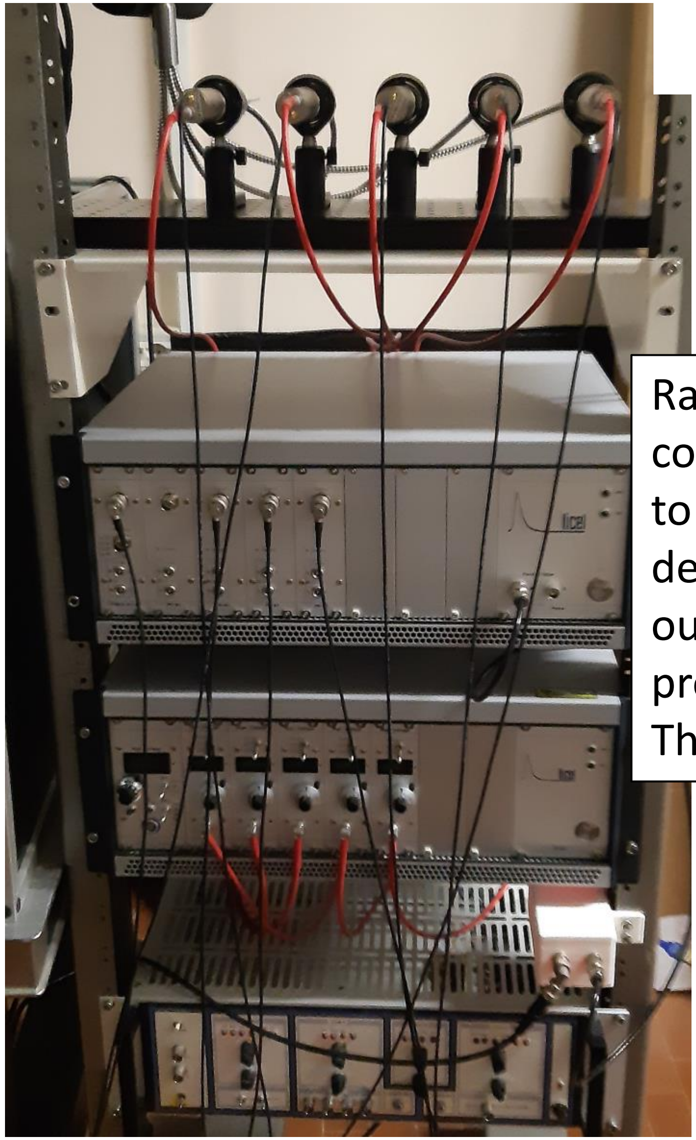

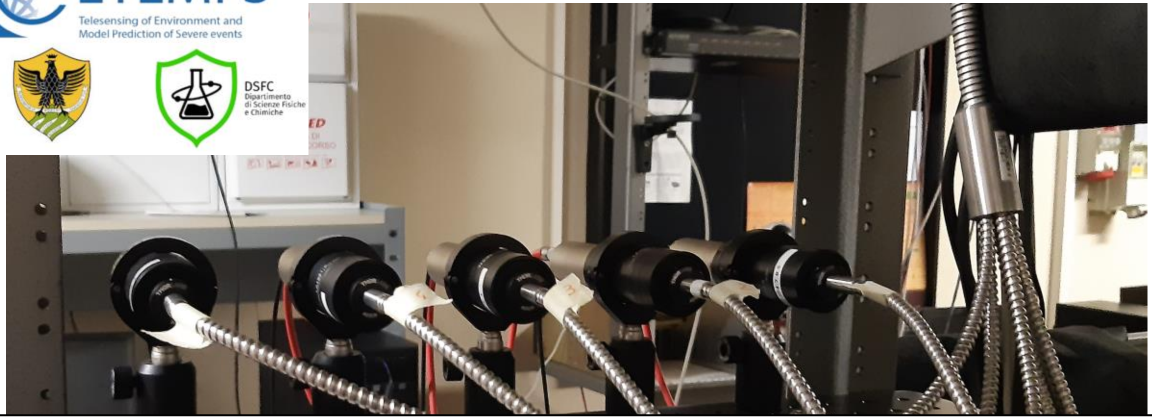

Raman LIDAR @ UNIVAQ: 3+2+d system that will allow a more complete characterization of aerosols since the system is able to measure optical properties (extinction and backscatter) and depolarization at different wavelengths; the measurements of our solar photometer and the molecular density profiles provided by our radiosondes will also be used for this purpose. This Lidar will operate within EARLINET/ACTRIS.

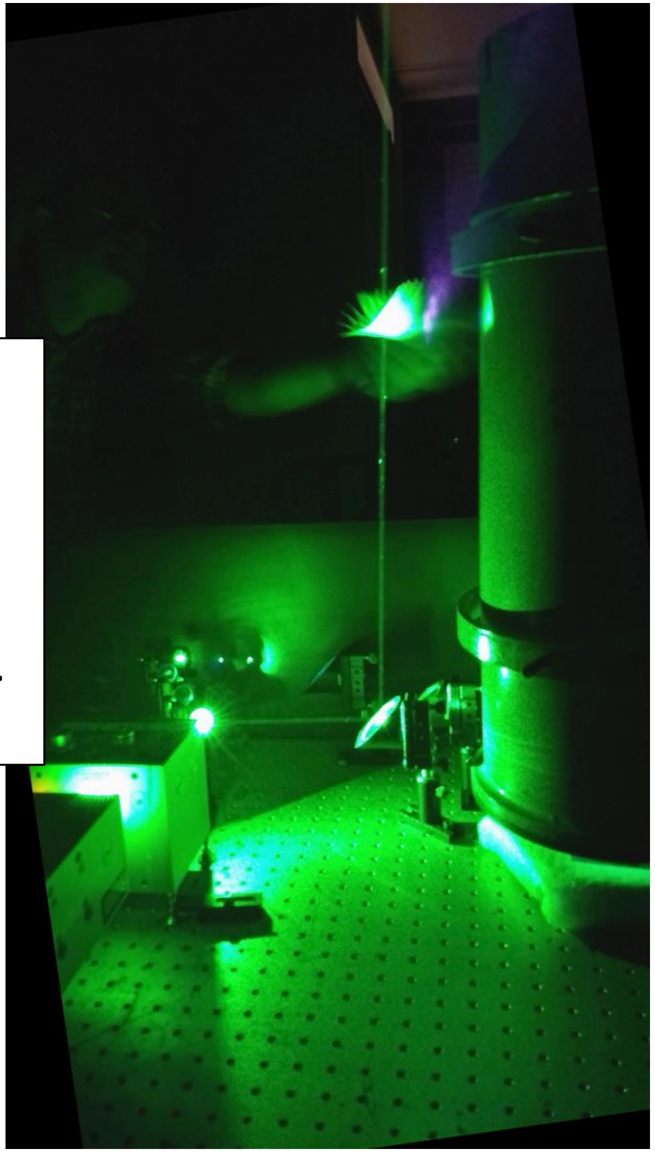


laser
optical
bench

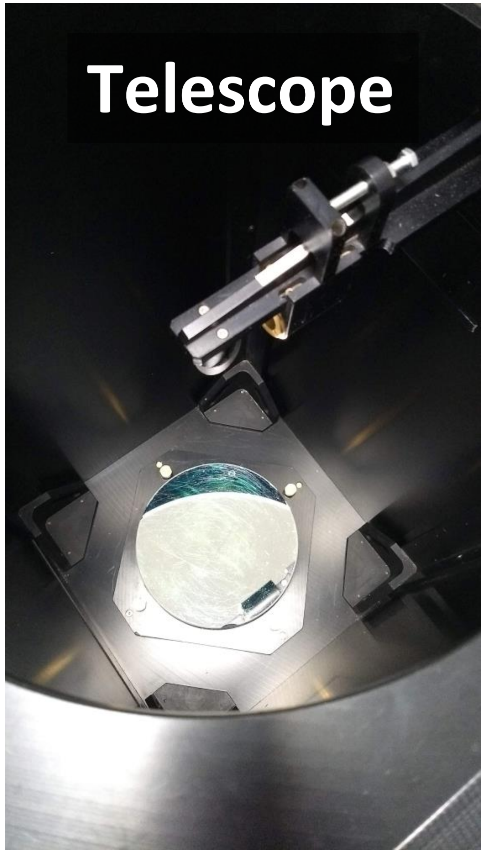
Telescope


Receiver
with PMTs

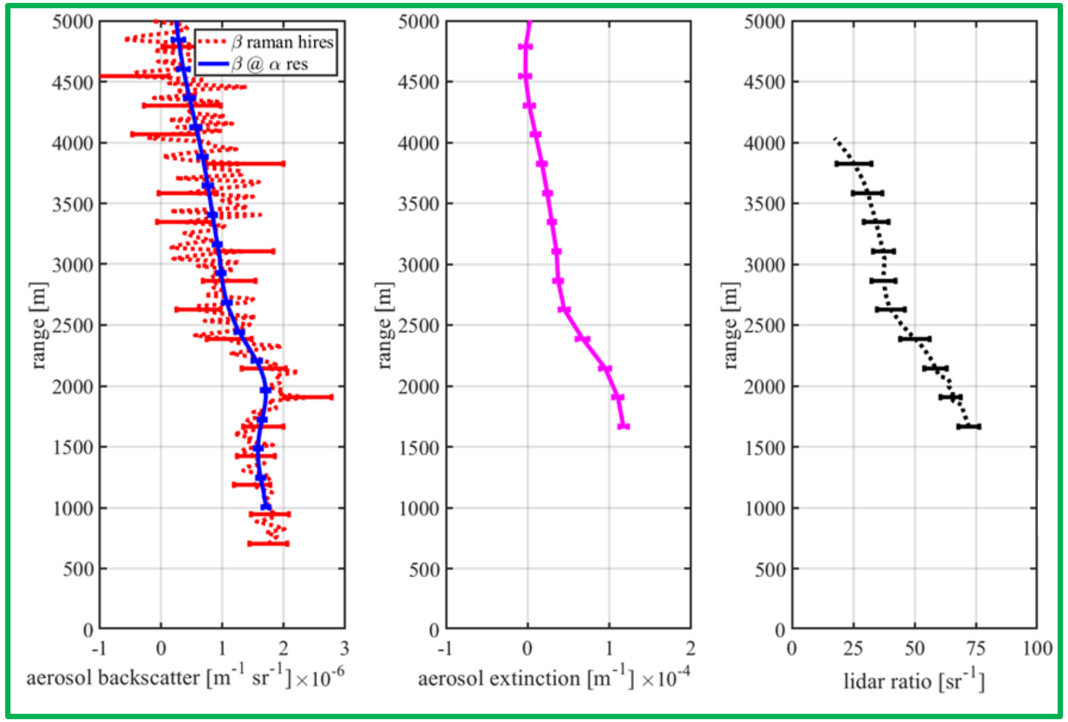
β raman hires
β @ α res
range [m]
aerosol backscatter [m^{-1} sr^{-1}] ×10^{-6}
aerosol extinction [m^{-1}] ×10^{-4}
lidar ratio [sr^{-1}]

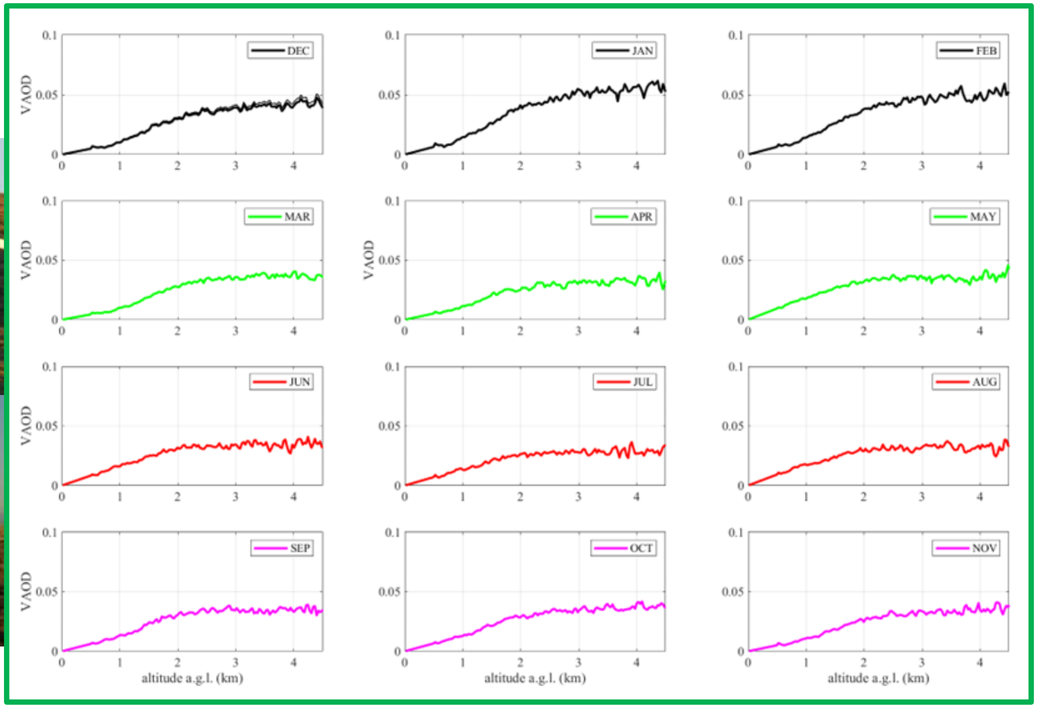
DEC
JAN
FEB
MAR
APR
MAY
JUN
JUL
AUG
SEP
OCT
NOV
VAOD
altitude a.g.l. (km)


HOME
INSTRUMENT
DATA
ARCADE
PUBLICATIONS
NEWS
GALLERY
cta
ARCADE Raman lidar
INFN
CETEMPS
Thank you!
PIERRE
AUGER
OBSERVATORY